

## INFORMATION TO USERS

This manuscript has been reproduced from the microfilm master. UMI films the text directly from the original or copy submitted. Thus, some thesis and dissertation copies are in typewriter face, while others may be from any type of computer printer.

**The quality of this reproduction is dependent upon the quality of the copy submitted.** Broken or indistinct print, colored or poor quality illustrations and photographs, print bleedthrough, substandard margins, and improper alignment can adversely affect reproduction.

In the unlikely event that the author did not send UMI a complete manuscript and there are missing pages, these will be noted. Also, if unauthorized copyright material had to be removed, a note will indicate the deletion.

Oversize materials (e.g., maps, drawings, charts) are reproduced by sectioning the original, beginning at the upper left-hand corner and continuing from left to right in equal sections with small overlaps. Each original is also photographed in one exposure and is included in reduced form at the back of the book.

Photographs included in the original manuscript have been reproduced xerographically in this copy. Higher quality 6" x 9" black and white photographic prints are available for any photographs or illustrations appearing in this copy for an additional charge. Contact UMI directly to order.

# U·M·I

University Microfilms International  
A Bell & Howell Information Company  
300 North Zeeb Road, Ann Arbor, MI 48106-1346 USA  
313/761-4700 800/521-0600



Order Number 9413299

**Interdecadal variability of the equatorial Pacific Ocean and  
atmosphere: 1930–1989**

Shriver, Jay Francis, Ph.D.

The Florida State University, 1993

**U·M·I**

300 N. Zeeb Rd.  
Ann Arbor, MI 48106



THE FLORIDA STATE UNIVERSITY  
COLLEGE OF ARTS AND SCIENCES

INTERDECADAL VARIABILITY OF THE EQUATORIAL PACIFIC  
OCEAN AND ATMOSPHERE: 1930-1989

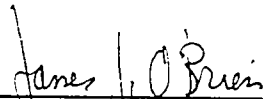
By

JAY F. SHRIVER

A Dissertation submitted to the  
Department of Meteorology  
in partial fulfillment of the  
requirements for the degree of  
Doctor of Philosophy

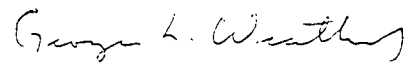
Degree Awarded:  
Fall Semester, 1993

The members of the Committee approve the dissertation of  
Jay F. Shriver defended on September 7, 1993.



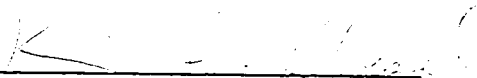
---

James J. O'Brien  
Professor Directing Dissertation



---

Georges L. Weatherly  
Outside Committee Member



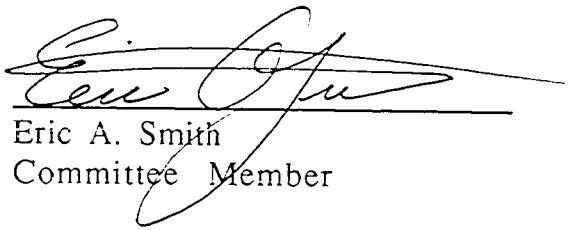
---

Kevin A. Kloesel  
Committee Member



---

Paul H. Ruscher  
Committee Member



---

Eric A. Smith  
Committee Member

## Acknowledgements

Nothing can survive in a vacuum and neither could have this dissertation. There are many people who deserve recognition for helping me throughout this project and I'd like to recognize their contributions.

I'd first like to thank professors Georges Weatherly, Paul Ruscher, Eric Smith and Kevin Kloesel for taking the time to be a part of my supervisory committee. Their comments, questions and suggestions were most useful.

Special thanks to mom and dad, without whom none of this would have been possible.

Thanks to my mom, Ian, Lisa and Maggie Palao and Rita and Kent Kuyper for helping me to maintain my sanity through the many times I thought I was going to lose it.

Thanks to Joe Fletcher at NOAA, conversations with whom prompted the work in this project.

Thanks to Dr. Steve Zebiak at Lamont Doherty for his invaluable technical assistance and thoughtful answers to questions I asked.

Thanks to Dr. Masa Kamachi. Besides being a good friend, Masa's modeling expertise and oceanographic insight made him a much valued resource.

Thanks to Dr. Brian Kelly, whose thoughtful proofreading of an earlier version of this dissertation helped correct several mistakes and made the manuscript more readable.

Special thanks are extended to my colleagues in the Mesoscale Air-Sea Interaction Group, both past and present, for always making me feel welcome and making my stay here in Tallahassee a pleasant one. You have all made my time here very enjoyable.

Finally I'd like to thank Dr. J. J. O'Brien, the man who made it possible for me to come to Florida State. Through my time at FSU, I was able to do many things I could never have hoped to do otherwise, and I have Dr. J. J. O'Brien to thank. He also taught me what it takes to do good research, something that I'm sure will prove invaluable throughout my career. Thanks el jefe.



## Table of Contents

	Page
LIST OF TABLES .....	vii
LIST OF FIGURES .....	viii
ABSTRACT .....	xiv
1. INTRODUCTION .....	1
2. DATA .....	8
2.1 PSEUDO-STRESS .....	8
2.1.1 COADS .....	8
2.1.2 FLORIDA STATE UNIVERSITY .....	8
2.2 SEA LEVEL .....	10
2.3 SEA SURFACE TEMPERATURE .....	15
3. SHIP TRACKS IN THE EQUATORIAL PACIFIC (1930-1989) .....	18
4. A METHOD FOR CREATING A CLIMATE DATA SET ....	25
5. MODEL .....	35
6. RESULTS AND DISCUSSION .....	39
6.1 FSU EOF ANALYSIS .....	39
6.2 SAMPLE ANALYSIS MONTH .....	39
6.3 DETRENDING .....	45
6.4 INTERANNUAL VARIABILITY .....	45
6.4.1 AVERAGE SST ANOMALIES .....	46

6.4.2 EOF ANALYSIS OF NEW PSEUDO-STRESS	
DATA SET .....	50
6.4.3 SEA LEVEL COMPARISONS .....	51
6.4.4 COMPARISONS WITH AVERAGE SST	
ANOMALIES .....	56
6.4.5 NORTH EQUATORIAL COUNTERCURRENT .....	59
6.4.6 COMPARISON WITH FSU FORCED RESPONSE ...	60
6.5 INTERDECADAL VARIABILITY .....	66
6.5.1 GLOBAL MEAN LAND AIR TEMPERATURE .....	66
6.5.2 EASTERN PACIFIC .....	68
7. SUMMARY AND CONCLUSIONS .....	73
APPENDIX A .....	77
APPENDIX B .....	79
APPENDIX C .....	81
APPENDIX D .....	83
REFERENCES .....	86
BIOGRAPHICAL SKETCH .....	91

## List of Tables

	Page
Table 1. El Niño years since 1930 as documented by Quinn <i>et al.</i> (1987). The classifications are as follows: W/M - near moderate, M - moderate, S - strong and VS - very strong.	14
Table 2. The model parameters used. The zonal resolution is defined as the grid distance between adjacent u and h points and the meridional resolution is defined as the grid distance between adjacent h and v points.	37
Table 3. The percent variances accounted for by the first 40 eigenmodes yielded by the EOF decomposition of the FSU pseudo-stress product.	40
Table 4. Years of El Niño events using the Japan Meteorological Agency criteria.	49

## List of Figures

	Page
Figure 1. Schematic showing regions in the Indo-Pacific region and surrounding continental areas with surplus or deficit precipitation during various phases of a typical El Niño. The phase of the El Niño is indicated in parentheses by a minus (antecedent year), zero (El Niño year) or plus (year following El Niño onset) (from Enfield, 1992).	2
Figure 2. Percent of COADS observations available as a function of time over the region of interest. The y axis represents the number of positions in the domain where at least one observation was available divided by the total number of positions in the domain (2155).	9
Figure 3. Island sea level stations used.	11
Figure 4. Monthly sea level anomalies from (a.) Galapagos (1960-1990) and (b.) Truk (1953-1983). The monthly sea level anomalies have been filtered using a 12-month moving average.	12
Figure 5. The average SST anomalies determined via the JMA criteria for the period 1930 - 1989.	17

Figure 6.	The distribution of COADS pseudo-stress observations for (a.) 1930-1934, (b.) 1935-1939 and (c.) 1940-1944. The size of the stars plotted are proportional to the number of months with at least 1 observation at that spatial position.	19
Figure 7.	The distribution of COADS pseudo-stress observations for (a.) 1945-1949, (b.) 1950-1954 and (c.) 1955-1959.	20
Figure 8.	The distribution of COADS pseudo-stress observations for (a.) 1960-1964, (b.) 1965-1969 and (c.) 1970-1974.	22
Figure 9.	The distribution of COADS pseudo-stress observations for (a.) 1975-1979, (b.) 1980-1984 and (c.) 1985-1989.	23
Figure 10.	The domain of the oceanic model used (124°E-76°W, 20°S-25°N). The picture corresponds to the model solution for 25 March 1985.	38
Figure 11.	The (a.) COADS observations for December 1962 (610 missing values) and (b.) the COADS observations for the same month subsampled to resemble the observation distribution of December 1934 (1516 missing values).	42

- Figure 12. The analyzed anomaly fields corresponding to (a.) the COADS observations for December 1962 and (b.) the COADS observations for the same month subsampled to resemble the observation distribution of December 1934. The difference between the fields depicted in (a.) and (b.) is shown in (c.). 43
- Figure 13. The root mean square discrepancy between the COADS observations and analyzed pseudo-stress anomalies for the period 1930-1989. the mean discrepancy is  $5.62 m^2s^{-2}$ . 44
- Figure 14. The number of positions in the area  $150^{\circ}W - 90^{\circ}W$  and  $4^{\circ}N - 4^{\circ}S$  where there was at least 1 observation. 48
- Figure 15. The first eigenmode's spatial pattern obtained from the EOF decomposition of the new pseudo-stress product. The first mode accounts for 41.29% of the variance. 52
- Figure 16. The time series which modulates the first eigenmode's spatial pattern. The average SST anomalies are plotted for comparison. 53
- Figure 17. The model sea level anomalies at a location corresponding to Galapagos and observed Galapagos sea level anomalies. The model sea level anomalies were formed by multiplying the model ULT anomalies by  $\frac{\Delta\rho}{\rho}$ . 55

Figure 18. The model upper layer thickness data at a location corresponding to Truk and observed Truk sea level.	57
Figure 19. The SST and ULT anomalies averaged over the area 150°W - 90°W, 4°N - 4°S.	58
Figure 20. Contours of zonal velocity at 140°W. The solid lines denote eastward velocities. Note the considerable variability in the position of the North Equatorial Countercurrent (mean position of approximately 6°N).	61
Figure 21. Interannual fluctuations in the model North Equatorial Countercurrent. The values plotted are obtained by averaging the $x$ velocity at 140°W between 3°N and 12°N. The average SST anomalies are plotted for comparison.	62
Figure 22. Time series of sea level differences across the North Equatorial Countercurrent in the central Pacific for the period 1950-1985 (from Wyrтки (1974), who later extended the time series to 1985).	63
Figure 23. The anomalous ULT fluctuations at a location corresponding to Galapagos vs. observed sea level anomalies. The model forcing in this case is the FSU pseudo-stress data set.	65

- Figure 24. Global mean land air temperature anomalies relative to 1951-1980 (Annual values and smoothed curves) (from *Oceanic Interdecadal Climate Variability, IOC Technical Series 40*. UNESCO, 1992). 67
- Figure 25. Low passed ULT and SST anomalies averaged over the area 150°W - 90°W, 4°N - 4°S. To filter periods less than 10-years, a Butterworth filter was used. 69
- Figure 26. Decadal average air-surface temperature or sea surface temperatures as departures from the 1951-80 mean, for 1977-86 (from Trenberth, 1990). 70
- Figure 27. Profile of zonally averaged temperature anomalies (°C) over both land and ocean areas during El Niño (solid line) and El Viejo (dashed line). The events composited span the period 1887-1988, using a classification criteria described in Kiladis and Diaz (1989). 72



## Abstract

Interannual and interdecadal variability of the equatorial Pacific is examined using a new 60-year monthly historical pseudo-stress data set. The monthly mean pseudo-stress fields (1930-1989) are assembled from Comprehensive Ocean-Atmosphere Data Set (COADS) pseudo-stresses using a variation of Cressman's (1959) objective analysis scheme, climate basis functions obtained from the FSU pseudo-stress product (1966-1990) and a technique called Vector Group Renormalization (VGR). The new wind fields are used to force an ocean model (Kubota and O'Brien, 1984). Model estimates of tropical Pacific current and model upper layer thickness (ULT) variability are then obtained for the period of interest. Observed sea level and spatially averaged sea surface temperature (SST) anomalies are used to validate the hindcasts.

Interannual fluctuations in modeled and observed sea level fluctuations are compared at Galapagos and Truk, yielding correlation ( $r$ ) values of 0.73 and 0.71, respectively. The comparison of the interannual fluctuations in modeled ULT and observed SST anomalies, which were both spatially averaged over a subdomain in the eastern Pacific basin, yielded a correlation ( $r$ ) value of 0.64.

Interdecadal fluctuations in eastern Pacific model ULT are found to be qualitatively consistent with those in the spatially

averaged observed SST anomalies. Interdecadal variations are shown to play a significant role in modulating the amplitude of El Niño events. Comparison of interdecadal fluctuations in global mean land air temperature and eastern Pacific ULT suggests a connection between eastern Pacific and global mean land air temperature warming for interdecadal time scales.

## 1. Introduction

El Niño is currently the most studied feature of global interannual variability. By definition, El Niño is the occurrence and persistence of anomalously high sea surface temperatures (SST) along the coast of Ecuador and Peru. The term El Niño is also used to represent anomalously high sea level and thermocline depression in the eastern Pacific, consistent and coincident with SST change (Busalacchi *et al.*, 1983). El Niño events are thought to decrease hurricane activity in the Atlantic, increase both droughts in southeast Asia and rainfall in parts of the Americas, and cause many other anomalous weather conditions (see Figure 1).

One key to our understanding of this phenomena was documented by Wyrtki (1975). El Niño was hypothesized to be a response of the equatorial Pacific Ocean to atmospheric forcing. In the tropical Pacific, prior to the onset of El Niño, strong trades exist over the central Pacific. The strong trades drive water to the western Pacific, increasing the east-west sea level slope. Relaxation of the trades then results in a decrease of the east-west sea level slope, accomplished through a downwelling equatorial Kelvin wave. The downwelling Kelvin wave yields a depressed thermocline and increased sea level in the eastern Pacific. This proposed dynamic mechanism for El Niño was given further credibility when a statistical analysis linked the variability of the zonal component of the southeast trades west of

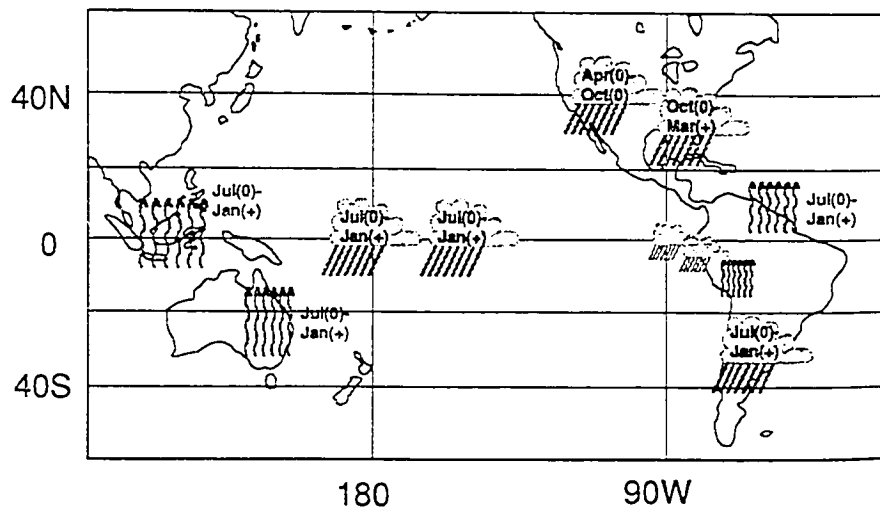


Figure 1. Schematic showing regions in the Indo-Pacific region and surrounding continental areas with surplus or deficit precipitation during various phases of a typical El Niño. The phase of the El Niño is indicated in parentheses by a minus (antecedent year), zero (El Niño year) or plus (year following El Niño onset) (from Enfield, 1992).

the dateline with sea level changes across the Pacific basin (Barnett, 1977).

In order to validate Wyrтки's hypothesis numerically, wind analyses of sufficient resolution to force an ocean model were necessary. Wyrтки and Meyers (1976) produced the first maps of time varying winds and wind stress over the Pacific Ocean for 1947-1972. This data set was on a rather coarse  $2^\circ$  longitude by  $10^\circ$  latitude grid which contained many data void regions as well as some obvious errors.

The Mesoscale Air-Sea Interaction Group at Florida State University chose to reanalyze the Wyrтки and Meyers wind data (Goldenberg and O'Brien, 1981). The analysis was performed on pseudo-stress (defined as the wind velocity vector multiplied by its magnitude) rather than the winds in order to produce wind stress fields for forcing ocean models. The three reasons for the reanalysis were:

- 1) to eliminate obvious errors in the Wyrтки and Meyers data set;
- 2) to yield a finer resolution data set, suitable for forcing ocean circulation models; and
- 3) to eliminate data void regions.

These Pacific wind analyses continue today (Stricherz *et al.*, 1992), using National Climatic Data Center (NCDC) global marine surface observations.

Busalacchi and O'Brien (1981) and Busalacchi *et al.* (1983) were the first to verify Wrytki's hypothesis numerically. They used a shallow water, reduced gravity, linear model on an equatorial beta ( $\beta$ ) plane. The forcing used was an estimate of Pacific wind stress (Stricherz *et al.*, 1992). The model simulations covered the period January 1961 through December 1978. Model pycnocline depth variations compared with observed sea level at Galapagos Island showed excellent agreement, both in timing and amplitude. This successful simulation of the El Niño events of 1963, 1965, 1969, 1972 and 1976 confirmed Wrytki's hypothesis.

Subsequent El Niño models have been developed by Barnett (1984), Inoue and O'Brien (1984) and Zebiak and Cane (1987) for use in forecasting El Niño occurrences. The basic characteristics of these models are different, even though all three use equatorial Pacific wind information. The models documented in Inoue and O'Brien (1984) and Zebiak and Cane (1987) are dynamic in nature, while Barnett (1984) used a statistical approach.

Previous modeling efforts have focused on the relatively data rich period from 1960's to the present (e.g. Busalacchi and O'Brien, 1981; Cane *et al.* 1986; Kubota and O'Brien, 1988). Bigg and Inoue (1992), however, ventured into the data poor period, investigating wind forced variability in 1935-1946. They were able to replicate reasonably observed eastern Pacific sea level trends. No one else has attempted to examine wind forced

variability over a time period longer than about 30 years, the approximate length of the relatively data rich 1960's to present.

A pseudo-stress data set which encompasses a longer period than the FSU data set would prove invaluable in the examination of tropical Pacific variability. Model simulations of wind forced equatorial Pacific variability could be conducted over a longer time period than that spanned by the FSU data set (1966-present), thereby increasing the ability to develop some insight into the low frequency variability of the ocean-atmosphere system.

In this research a pseudo-stress data set is compiled for the period 1930-1989. The monthly mean pseudo-stress fields are assembled from Comprehensive Ocean-Atmosphere Data Set (COADS) pseudo-stresses using a variation of Cressman's (1959) objective analysis scheme and a technique called Vector Group Renormalization (VGR). Using an equatorial Pacific model (Inoue and O'Brien, 1984), model estimates of tropical Pacific current and model upper layer thickness (ULT) variability are obtained for the period of interest. Historical documentation of El Niño events (Quinn *et al.*, 1987), spatially averaged sea surface temperature (SST) and equatorial Pacific sea level data are then used to validate the model hindcasts. Interannual and interdecadal fluctuations in model ULT and the North Equatorial Countercurrent (NECC) are also examined and compared with observations.

An area of intense research recently is global climate change. Analysis of global mean land air temperature shows considerable interannual and interdecadal variability superposed upon an upward trend which persists throughout the 20th century. Is this increase in temperature part of a global warming trend due to increases in atmospheric CO<sub>2</sub>, or natural decadal scale fluctuations? Only by developing a better understanding of climatic fluctuations on decadal time scales will man's influence on climate be put into the proper perspective.

In this research interdecadal fluctuations were found to play a major role in eastern Pacific Ocean variability. These fluctuations are shown to play a major role in modulating the amplitude of El Niño events. Previous work has shown a connection between eastern tropical Pacific Ocean and global mean land air temperature warming for El Niño variability (Diaz and Kiladis, 1992). My model results suggest that the connection between global air temperature and eastern Pacific warming holds for interdecadal variability as well.

Other uses for this new pseudo-stress data set include deriving equatorial Pacific sea surface temperature distributions through the use of an equatorial Pacific model with thermodynamics and examining mid-latitude Pacific variability caused by coastal Kelvin waves (e.g. Johnson and O'Brien, 1990; Shriver *et al.*, 1991). Using data assimilation techniques, it would



be possible to assimilate observed ocean temperatures into the hindcasted SST field to actually improve the wind set.

The next section discusses the SST, sea level and pseudo-stress data used in this research. Section 3 examines the variations in the observation patterns over the equatorial Pacific for 1930-1989. Section 4 develops the technique used to form the new pseudo-stress data set. Section 5 will present the model used. Section 6 will present and discuss the results. The last section is devoted to my conclusions.

## 2. Data

### 2.1. *pseudo-stress data sets*

#### 2.1.1. COADS

The COADS data set (Slutz *et al.*, 1985) covers the period 1854 to the present with global spatial coverage. The wind observations in this data set are compiled from ship data and buoys. Some basic quality control is performed so that duplicates and statistical outliers are removed. The threshold used to determine statistical outliers was 3.5 standard deviations from the median. Monthly mean values are formed and then gridded on a 2° by 2° mesh. The domain of interest covers 29°N-29°S, 124°E-70°W, lending to 2155 possible positions where observations could be taken. A plot of available observations over time is shown in Figure 2. Between 70% and 80% of the positions in the domain have at least one observation for 1960-1990, tailing off to about 20% by 1950. With the exception of two surges in the number of observations in the mid 1930's and 1940's, the number of grid points with observations decreases to less than 20% towards the beginning of the century.

#### 2.1.2. *Florida State University (FSU)*

The FSU pseudo-stress data set (Stricherz *et al.*, 1992) consists of monthly fields which span the period 1966 to the present, with spatial coverage from 124°E-70°W and 29°S-29°N.

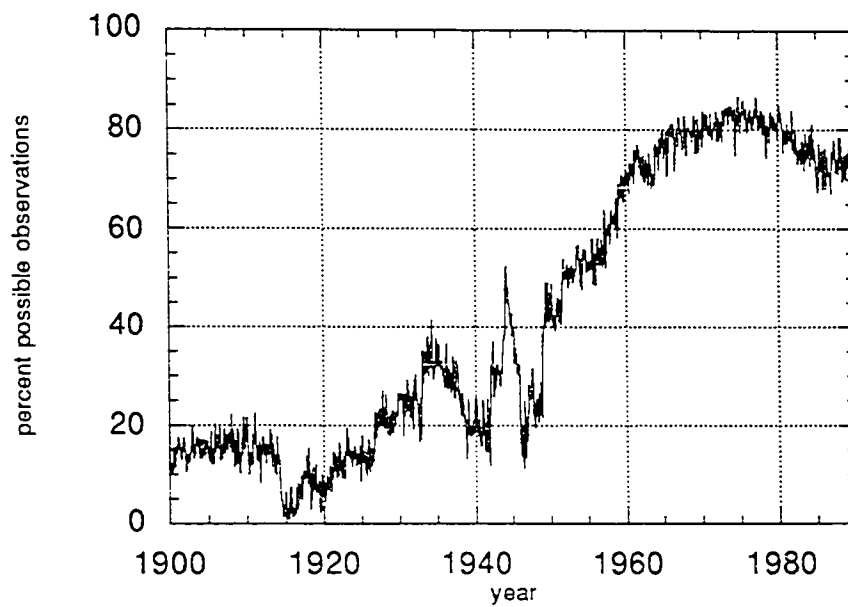


**Figure 2.** Percent of COADS observations available as a function of time over the region of interest. The y axis represents the number of positions in the domain where at least one observation was available divided by the total number of positions in the domain (2155).

The data are gridded on a  $2^\circ$  by  $2^\circ$  spatial grid. The analyses for the period 1966-1980 are based on individual ship reports obtained from the COADS data set. The analyses from 1981-present are based on NCDC global marine surface observations.

## 2.2. sea level

The sea level data used are from Galapagos (1960-1990) and Truk (1947-84). The locations of Truk and Galapagos are shown in Figure 3. Galapagos is located at approximately  $90^\circ\text{W}$ ,  $.5^\circ\text{S}$  and Truk is located at  $7.5^\circ\text{N}$ ,  $152^\circ\text{E}$ . These two positions are chosen due to their locations on opposite sides of the equatorial Pacific basin. The sea level data used are monthly averages. The Galapagos sea level data were provided by Klaus Wyrtki and the Truk sea level data were obtained from the Permanent Service for Mean Sea Level (PSMSL) data set.

Figure 4(a.) shows coastal sea level for Galapagos. The monthly climatology has been removed and a 12-month moving average has been applied to highlight the interannual variability. The El Niño events, indicated by peaks in sea level, are consistent in terms of relative amplitude and timing with the events documented by Quinn *et al.* (1987) (see Table 1). The immense magnitude of the largest El Niño event of the century, 1982-1983, is readily apparent.

Figure 4(b.) shows coastal sea level for Truk (climatology removed, 12 month moving average applied). Truk sea level data

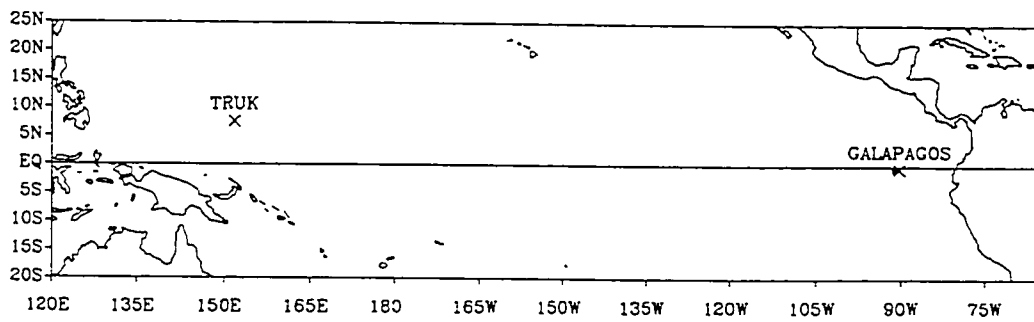
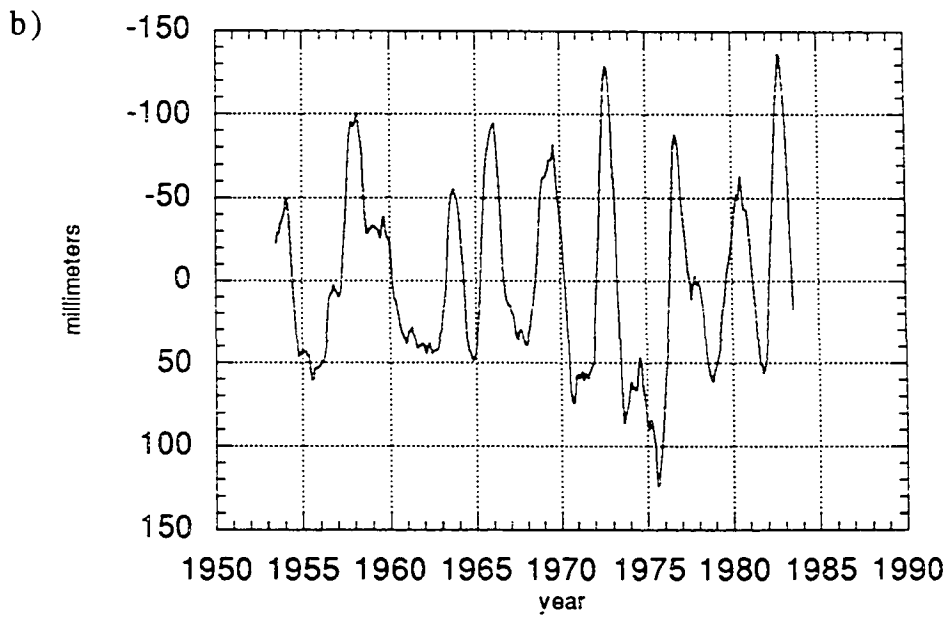
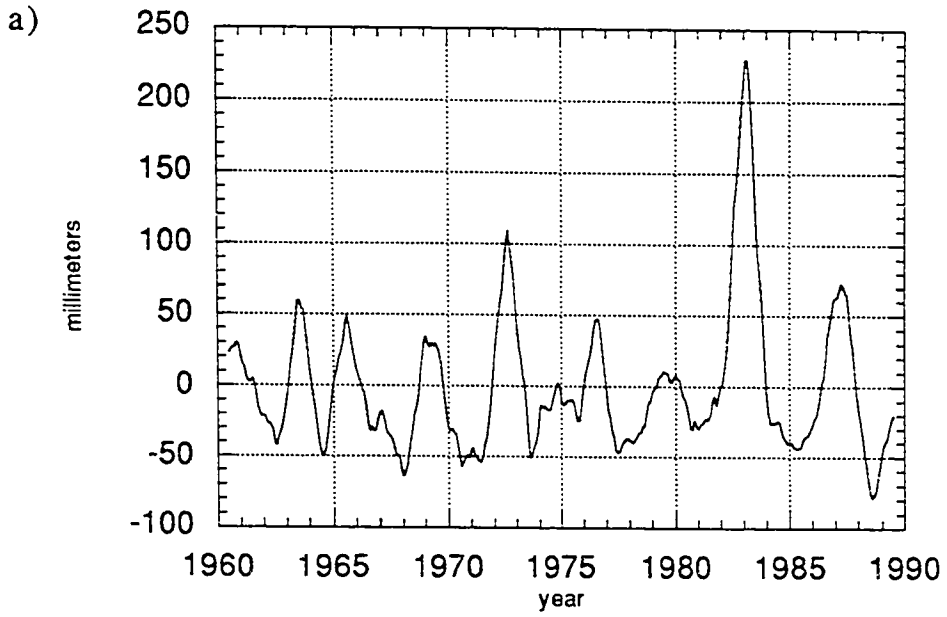


Figure 3. Island sea level stations used.

**Figure 4.** Monthly sea level anomalies from (a.) Galapagos (1960-1990) and (b.) Truk (1953-1983). The monthly sea level anomalies have been filtered using a 12-month moving average.



**Table 1.** El Niño years since 1930 as documented by Quinn *et al.* (1987). The classifications are as follows: W/M - near moderate, M - moderate, S - strong and VS - very strong.

El Niño years	event strength
1930 - 31	W/M
1932	S
1939	M+
1940 - 41	S
1943	M+
1951	W/M
1953	M+
1957 - 58	S
1965	M+
1972 - 73	S
1976	M
1982 - 83	VS
1987	M



are available for the period 1947-84, but in continuous form only for 1953-84 (with the exception of 2-month gaps in 1955 and 1975, which were both filled using linear interpolation). The y axis in Figure 4(b.) has been reversed so that peaks in the curve correspond to El Niño years. The wind changes near the dateline which trigger El Niño excite downwelling Kelvin waves which increase sea level at Galapagos and upwelling Rossby waves which decrease sea level at Truk. The fluctuations in Galapagos sea level are mirrored in Figure 4(b.), with a sea level fall coinciding with the El Niño of 1957-1958 also being depicted.

### *2.3. sea surface temperature*

The Japan Meteorological Agency (JMA) defines El Niño and its period as follows:

- (1.) Calculate monthly SST anomalies averaged for the area 4°N to 4°S and 150°W to 90°W.
- (2.) The periods in which the 5-month running mean of SST anomalies in this area is at least +.5°C for a minimum of 6 consecutive months is termed an El Niño.

The 5-month running mean of SST anomalies is implemented to smooth out possible intraseasonal variations.

The JMA implemented the above analysis for the period 1949-92. However, average SST data were needed prior to 1949 for this research. Using available COADS observations, SST values

averaged over the area  $4^{\circ}\text{N}$ - $4^{\circ}\text{S}$ ,  $150^{\circ}\text{W}$ - $90^{\circ}\text{W}$  were formed for the period 1930-1989. The monthly means were then removed and a 5-month moving average was applied. The resultant time series is shown in Figure 5. The interannual fluctuations in SST are consistent with those in the island sea level figures shown earlier.

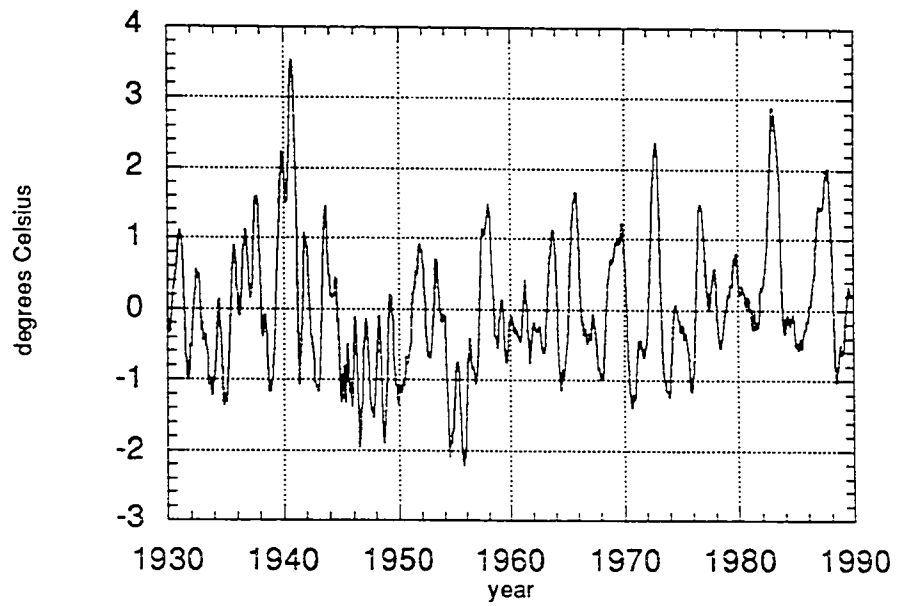


**Figure 5.** The average SST anomalies determined via the JMA criteria for the period 1930 - 1989.

### **3. Ship Tracks in the Equatorial Pacific (1930-1989)**

Almost all of the COADS pseudo-stress data for the period 1930-1989 were based on ship observations. As Figure 2 shows, there is large temporal variability in number of observations in the equatorial Pacific, but there is large spatial variability as well. This section will examine the changing ship traffic patterns over the equatorial Pacific by examining each 5-year period from 1930-1989.

The 1930's (Figures 6(a.) and (b.)) show high ship traffic in the Philippine Sea and near the coastlines on either side of the basin, with several well defined ship tracks being evident: western US - southwest Pacific basin, western US - Hawaii, Hawaii - Eastern Asia and Hawaii - Fiji. The influence of the Panama Canal on shipping is readily apparent, with well defined shipping lanes between the canal and Fiji and points southwest. During the second half of the decade, the Panama Canal traffic shows a significant decrease in traffic while the Philippine Sea traffic shows an increase.

World War II's influence on shipping patterns during the 1940's is clearly evident (Figures 6(c.) and 7(a.)). The shipping tracks from the late 1930's persist, but there is a significant decrease in traffic and the lanes become less defined. In the second half of the decade the high traffic in the Panama Canal - Southwest Pacific basin shipping lanes resumes and shipping in

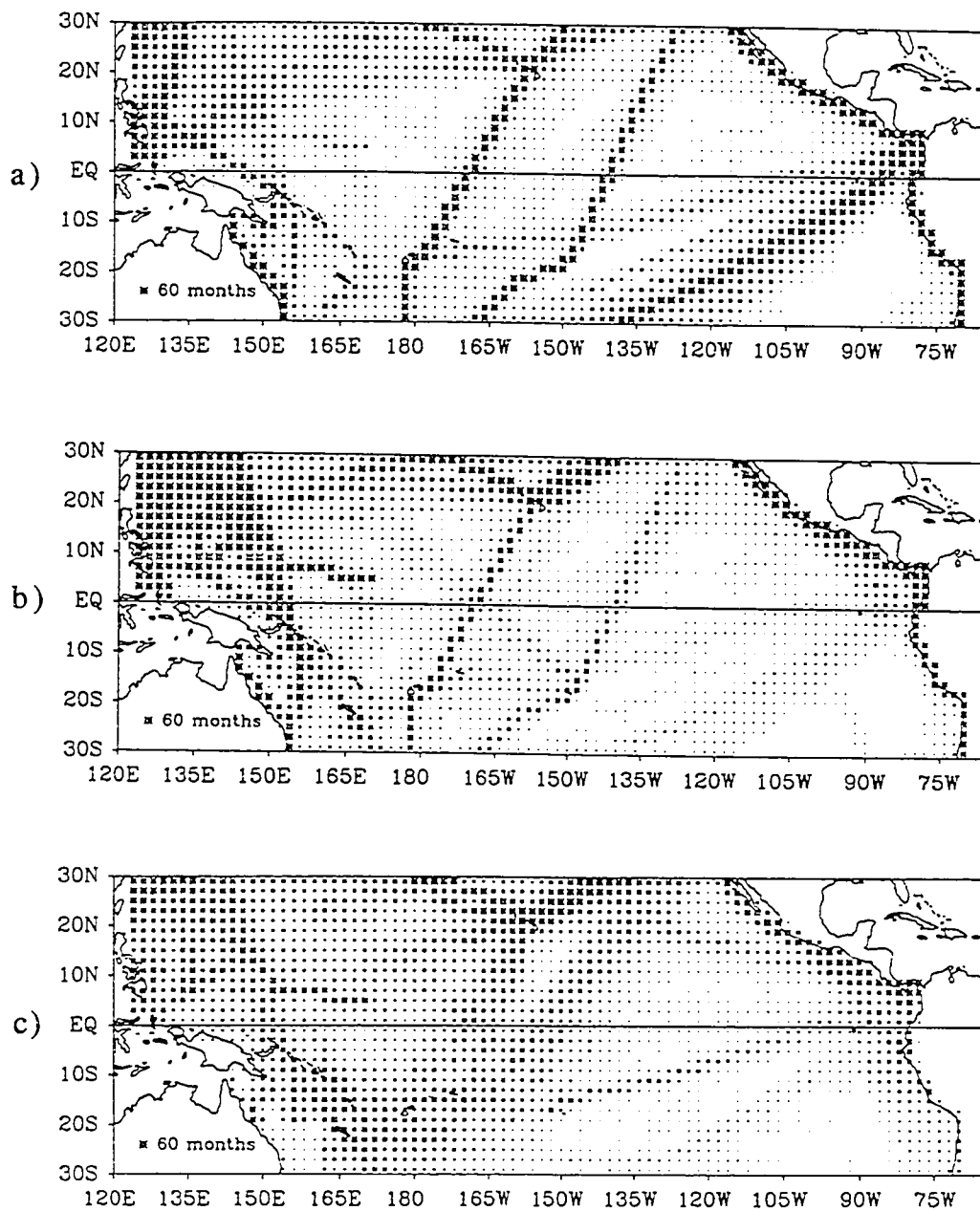
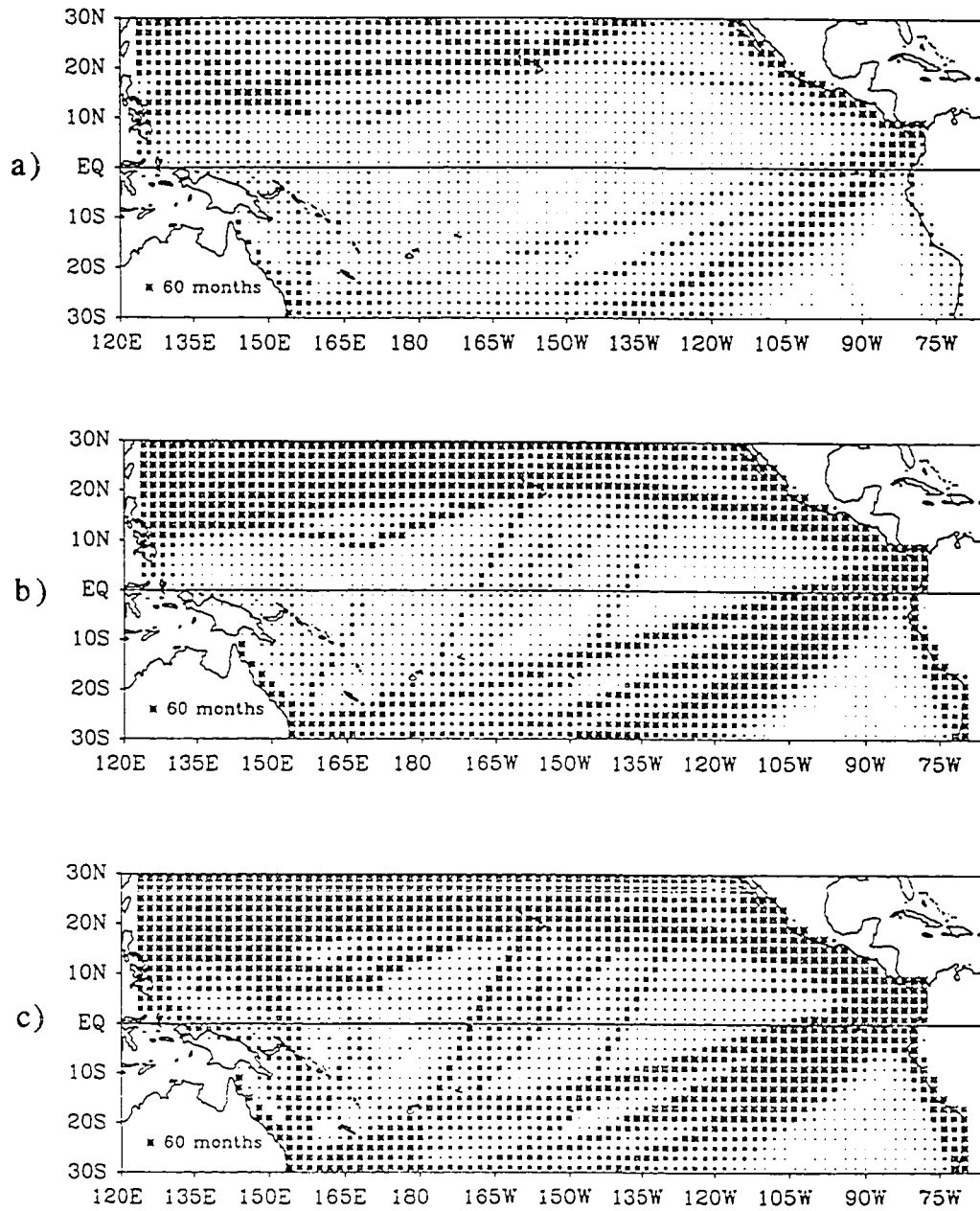


Figure 6. The distribution of COADS pseudo-stress observations for (a.) 1930-1934, (b.) 1935-1939 and (c.) 1940-1944. The size of the stars plotted are proportional to the number of months with at least 1 observation at that spatial position.



**Figure 7.** The distribution of COADS pseudo-stress observations for (a.) 1945-1949, (b.) 1950-1954 and (c.) 1955-1959.

the North Pacific increases. Cross-equatorial shipping, however, shows a significant drop.

The 1950's (Figures 7(b.) and (c.)) show a general increase in traffic, with a return of cross-equatorial shipping. The Panama Canal and north Pacific traffic show large increases. The well defined shipping lanes between Fiji - Hawaii and western USA - Southwest Pacific return, and they show an increase in traffic in the second half of the decade. There is also an increase in Coral Sea and far western Pacific cross-equatorial observations during the second half of the 1950's.

The growth of the number of observations starts to level off in the 1960's (Figure 2). The increase in Coral Sea and far western Equatorial Pacific observations continues in the early 1960's (Figures 8(a.) and (b.)). The number of observations in the central equatorial and south Pacific have also increased.

In the 1970's the number of observations peak and there is a slight decrease by the end of the decade (Figure 2). Spatially, the observation patterns from the 1960's continue, with an increase in the number of observations near the dateline (Figures 8(c.) and 9(a.)). There is also an increase in ship traffic from the South American coast into the Central Pacific.

By the end of the 1980's the total number of observations has decreased by about 10% (Figure 2). There are sizable decreases in observations along the South American coast - Central Pacific and Panama Canal - Southwest Pacific shipping lanes (Figures 9(b.) and (c.)).

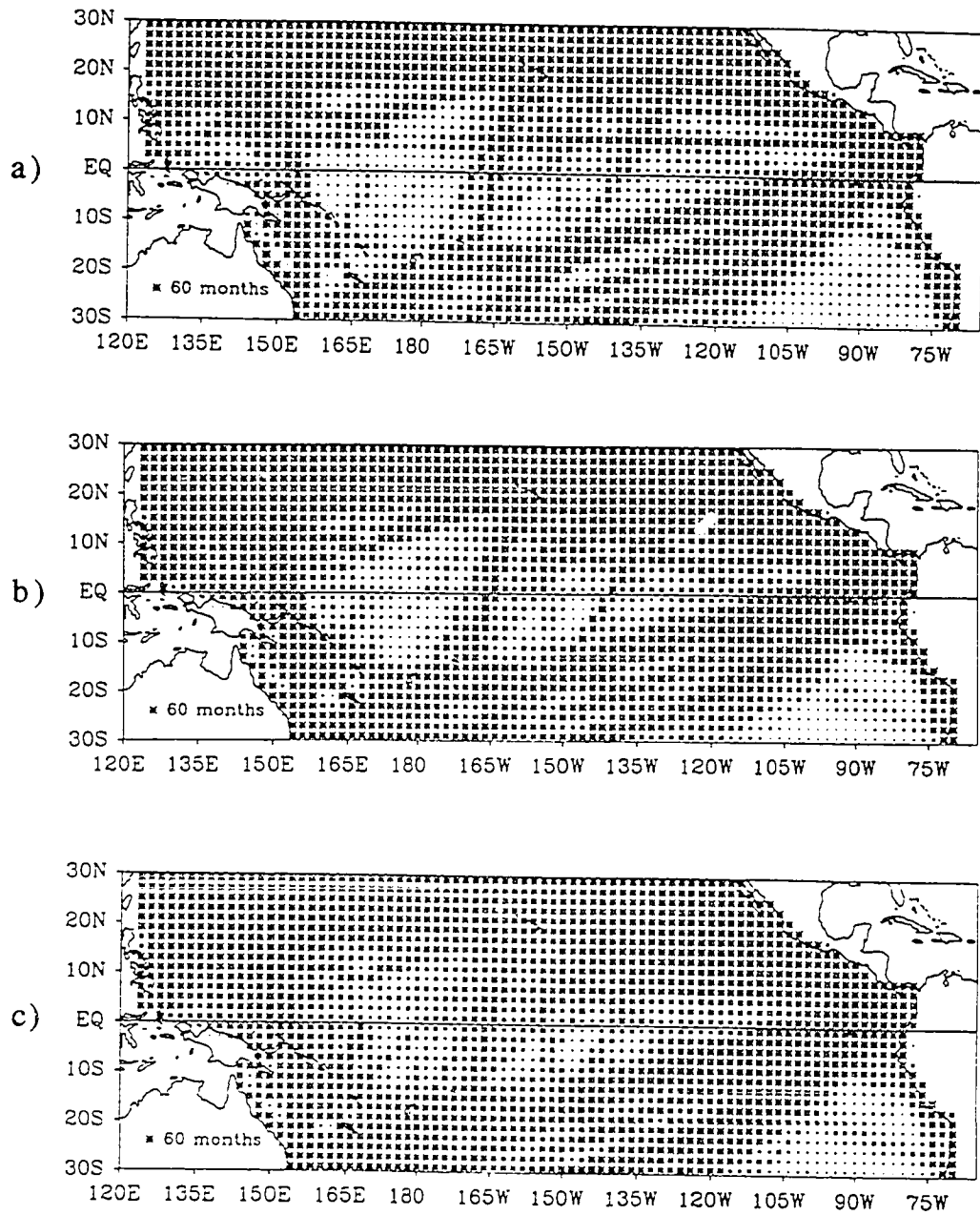


**Figure 8.** The distribution of COADS pseudo-stress observations for (a.) 1960-1964, (b.) 1965-1969 and (c.) 1970-1974.



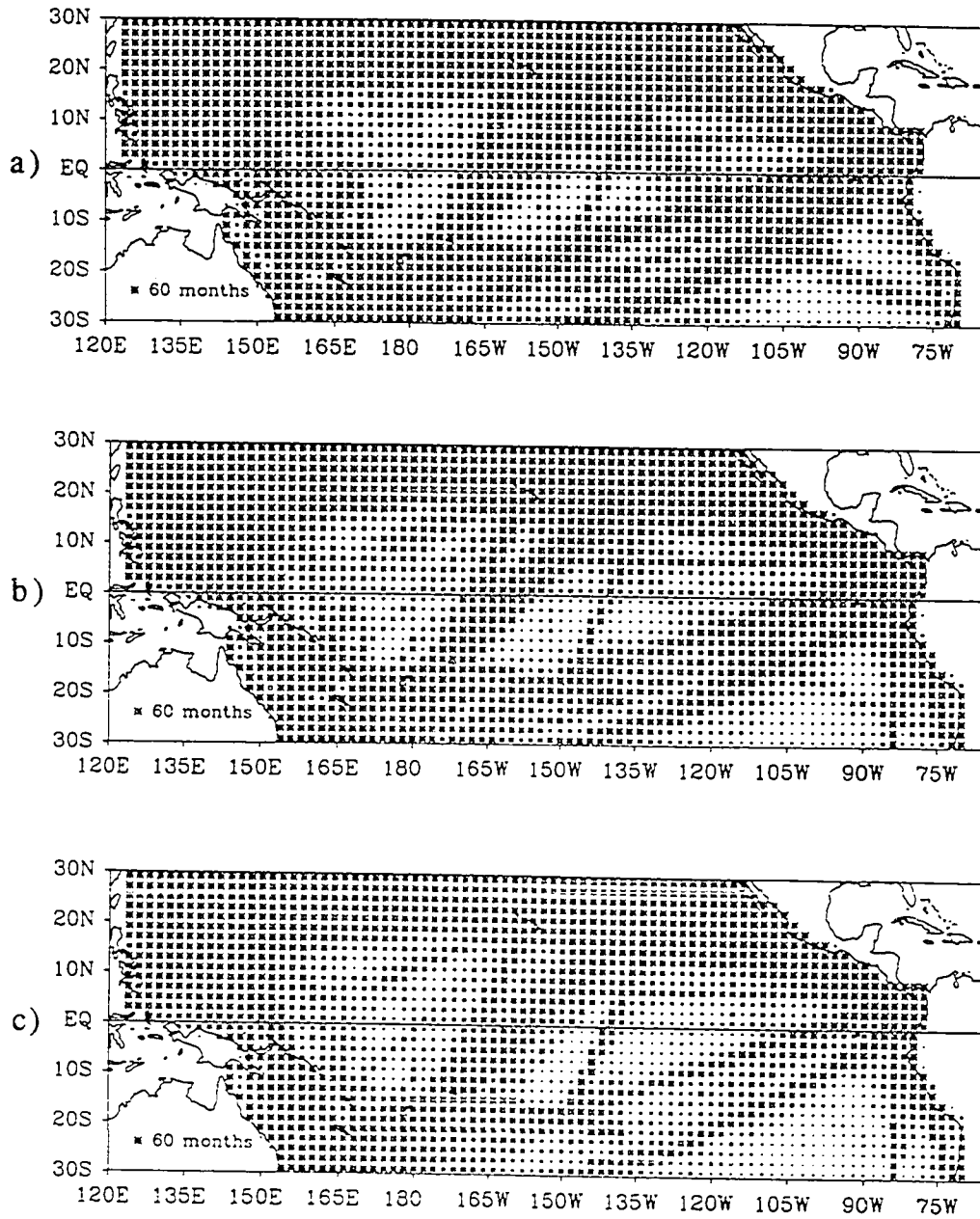


**Figure 9.** The distribution of COADS pseudo-stress observations for (a.) 1975-1979, (b.) 1980-1984 and (c.) 1985-1989.

In summary, the Pacific Ocean ship-based observations are dominated by 5 sources:

- 1.) near-coast ship traffic
- 2.) the Panama Canal - southwest Pacific shipping lanes
- 3.) Pacific ship traffic hubbing out of Hawaii
- 4.) western US - southwest Pacific shipping lanes.
- 5.) Philippine Sea traffic.

The geographical constraining of most of the ship traffic to the above areas ultimately leads to several regions of the equatorial Pacific having little or no wind observations, most notably:

- 1.) the southeast corner of the domain
- 2.) the southern hemisphere
- 3.) along the equator.

#### **4. A Method for Creating a Climate Data Set**

This chapter will develop the technique used to form the new 60-year pseudo-stress data set. The new data set will be derived from the observed COADS pseudo-stress. The sparse COADS coverage, particularly before 1960, necessitates an objective analysis scheme which incorporates physical constraints to overcome the analysis problems that very sparse data coverage poses.

Model studies have demonstrated that western Pacific wind anomalies appear to initiate El Niño (Enfield, 1989). The period spanned by the FSU data set (1966-1990) contains 5 El Niño events (1969, 1972, 1976, 1982-83 and 1986). The physics which drive these events are consistent from event to event. This consistency allows a simple statistical model such as that by Barnett (1984) to be able to predict El Niño several months in advance. It would then be reasonable to expect that the wind fields which forced the 5 El Niño events within this period contain a significant portion of the spatial variability which would be needed to reproduce the El Niño events prior to 1966.

Dominant spatial patterns for the period 1966-1990 (termed climate basis functions) can be determined through a vector EOF analysis of the FSU Pacific wind stress product. Since the spatial variability contained within the climate basis functions is expected to be sufficient to reproduce the El Niño events for

1930-1989, desired wind fields for this period can then be represented as the superposition of this set of climate basis functions (each modulated by a certain time coefficient). The method used to solve for these time coefficients will be developed later in this chapter.

The FSU Pacific wind stress product (1966-1990) is analyzed using vector EOF analysis (see Appendix A for a discussion of this technique). Let  $\mathbf{w} = \mathbf{T}_x + i\mathbf{T}_y$ , where  $\mathbf{w}$ ,  $\mathbf{T}_x$  and  $\mathbf{T}_y$  are each 2155 (spatial positions) by 300 (months) matrices and  $i = \sqrt{-1}$ . The matrices  $\mathbf{T}_x$  and  $\mathbf{T}_y$  represent the eastward and westward components of the FSU pseudo-stress product, respectively. Before EOF processing, the climatological monthly means from  $\mathbf{T}_x$  and  $\mathbf{T}_y$  are removed. The EOF decomposition of  $\mathbf{w}$  yields 300 pairs of space-time vectors  $Z$  and  $M$ .

I next wanted to isolate the statistically significant spatial patterns yielded by the FSU vector EOF analysis. The significant patterns are determined using a statistical test (Overland and Preisendorfer, 1982). Spatial patterns are determined to be not significant if the eigenvalue corresponding to that spatial pattern is less than one generated from a random data set (see Appendix B for details). The set of  $K$  statistically significant spatial patterns ( $K=40$ ) will then be referred to as the climate basis functions set.

The climate basis functions set, along with COADS winds, can now be used to determine complete wind fields for the years prior to 1966. Let the matrix  $T$  represent the COADS data. Since the climate basis functions were derived from wind fields where

the monthly climatology was removed, the monthly climatology must also be removed from T. A question then arises, how should the monthly climatology which will be removed from T be defined?

The calculation of a monthly climatology from T for the period 1930-1989 would produce a product where the representativeness would vary due to spatial and temporal variations in the distribution of observations. The FSU monthly climatology is another data set which could be used to demean T. However, the use of the FSU climatology to demean the COADS data is equivalent to stating that the climatology hasn't changed significantly over the equatorial Pacific.

The idea that climatology over the equatorial Pacific hasn't changed significantly over the period 1930-1989 is certainly a nontrivial assumption. How valid is it? A two-tailed t-test was used, using 95% confidence limits, to see if the null hypothesis that the FSU climatology was the correct climatology for 1930-1989 could be rejected. If the FSU climatology is the proper climatology for the period of interest, then an alternative statement of the null hypothesis would be that the monthly mean COADS departures from the FSU climatology are zero. The alternative null hypothesis is what was actually tested (see Appendix C for details). Approximately 85% of the time the null hypothesis could not be rejected. The FSU climatology is then used to demean the COADS data.

There are often large regions in T where no data are available, since the wind observations come from either ship tracks or buoys. My goal is to fill these gaps in T so the resultant wind fields can be used to examine certain aspects of the climate, specifically occurrences of El Niño.

A variation of Cressman's (1959) objective analysis scheme is first applied to the COADS anomalies to smooth the values at positions with data and to interpolate values (if possible) at positions without data. As originally put forth, the weights for this scheme are radially symmetric. In the equatorial Pacific, east-west length scales are longer than north-south scales (e.g. Kubota and O'Brien, 1988) therefore it is expected that the weight contours should resemble ellipses, not circles.

The weights are determined as follows: using the FSU data set, where the monthly means have been removed, lag correlations ( $r^2$ ) are calculated first for each north-south line for each month, yielding an autocorrelation matrix  $acf1(x, ylag, t)$ , where  $x$  is the longitudinal grid position,  $ylag$  is the north-south lag and  $t$  is the time index. The same is then done for each east-west line yielding a matrix  $acf2(y, xlag, t)$ , where  $xlag$  is the east-west lag and  $y$  corresponds to the latitudinal grid position. The functions  $acf1$  and  $acf2$  are then averaged to yield monthly average autocorrelation matrices  $\hat{acf1}(x, ylag, m)$  and  $\hat{acf2}(y, xlag, m)$ , where  $m=1, 2, \dots, 12$  (Jan., Feb, ... , Dec.). I then define a weight matrix  $acf$  as follows:

$$\text{acf}(x, y, m; x_0, y_0) = \exp\left(-\left(\frac{(x-x_0)^2}{\gamma(y, m)^2}\right) - \left(\frac{(y-y_0)^2}{\Delta(x, m)^2}\right)\right)$$

where  $x_0$  and  $y_0$  correspond to the position where either an existing value is being smoothed or a value is being interpolated and  $x$  and  $y$  correspond to some neighboring position. The e-folding matrix  $\Delta(x, m)^2$  is defined as the  $(y-y_0)^2$  distance in which  $\hat{\text{acf}}_1$ , for fixed  $x$  and  $m$ , decreases to  $e^{-1}$ . The e-folding matrix  $\gamma(y, m)^2$  is defined as the  $(x-x_0)^2$  distance in which  $\hat{\text{acf}}_2$ , for fixed  $y$  and  $m$ , decreases to  $e^{-1}$ . Any acf values less than  $e^{-2}$  are set to zero.

The algorithm used for the scan is as follows: at first I calculate

$$\hat{T}(x_0, y_0, t) = \sum_x \sum_y \text{acf}(x, y, m; x_0, y_0) \text{nobs}(x, y, t) T(x, y, t) \quad (1.)$$

where  $T(x, y, t)$  is the COADS observation and  $\text{nobs}(x, y, t)$  is the number of observations at position  $(x, y)$  and time  $t$ . After one pass of the entire data set,  $\hat{T}$  is then smoothed in time at each spatial position using one  $\frac{1}{4} - \frac{1}{2} - \frac{1}{4}$  weighting Hanning pass.

The desired pseudo-stress product can be represented as a superposition of the climate basis functions by the following:

$$Y = Z\alpha \quad (2.)$$

where  $Y$  is a column vector of length 2155 (spatial positions), representing a complete wind field. The matrix  $Z$  is a 2155 (spatial position) by  $K$  (number of spatial patterns) matrix, where the column vectors of  $Z$  constitute the set of climate basis functions. The column vector  $a$  contains the  $K$  unknown modulation coefficients. Note that the procedure used is done for a particular month  $t$  and that each monthly wind field  $Y$  is solved for independently.

How can a solution for  $a$  be obtained? Determining the discrepancy between (2.) and  $W$  is straightforward. The column vector  $W$  is of length 2155 (spatial positions) and has the values yielded by (1.) for a month  $t$  mapped into it. Weights related to the number of observations at a given point can also be incorporated. This leads to the following discrepancy sum which I would want to minimize

$$D = |HW - HZx| \quad (3.)$$

where  $H$  is a square diagonal matrix of order 2155 (spatial positions) with weights  $\alpha_s$  on the diagonal and  $x$  is an arbitrary solution vector of length  $K$ . The weights  $\alpha_s$  are equal to the number of observations at position  $s$  if  $W_s$  (corresponding to an element of  $W$ ) is a smoothed value, 1 if  $W_s$  is an interpolated value or 0 if  $W_s$  is missing. The notation  $|j|$  denotes the Euclidean norm of  $j$ .



In order to solve for the optimal solution vector  $a$  which minimizes (3) it can be shown that the vector  $(HW - HZa)$  must be orthogonal to all vectors of the form  $HZx$ . This implies that  $(HW - HZa)$  is orthogonal to all column vectors of  $HZ$ , i.e.

$$(HZ)^*{}^T(HW - HZa) = 0.$$

Using the definition of transpose the above equation can be rewritten as

$$Z^*{}^T \hat{H} W = Z^*{}^T \hat{H} Z a \quad (4.)$$

where  $\hat{H} = H^*{}^T H$ . The square matrix  $\hat{H}$  is a diagonal matrix with weights  $\alpha_i^2$  on the diagonal. The optimal solution vector  $a$  can be expressed as

$$a = (Z^*{}^T \hat{H} Z)^{-1} Z^*{}^T \hat{H} W.$$

Through the minimization of (3.) I can solve for the time coefficients  $a$  which modulate each of the climate basis functions,  $Z_{s,k}$  for the month(s) of interest. Using (2.) I then obtain pseudo-stress fields. Note that because of the assumptions which were made about the Equatorial Pacific wind field, the task of forming complete wind pictures reduces to solving a weighted least squares problem.

A technique called Vector Group Renormalization (VGR) is used (see Appendix D) in order to solve (4.) for the optimal solution vector  $a$ . This technique is an alternative way to obtain  $a$  without having to invert a matrix.

Now applying VGR to my case I first transform the matrix  $Z$  into a new matrix  $Z'$  such that product of any two column vectors  $Z'_j$  and  $Z'_k$ , which are the  $j$ th and  $k$ th columns of  $Z'$ , satisfies the following product rule

$$\langle Z'_j, Z'_k \rangle = Z_j^T \hat{H} Z_k^* \quad (5.)$$

where the result is equal to 1 if  $j=k$  or 0 otherwise. Next, I then take the complex conjugate of both sides of equation (4.), yielding

$$Z^T \hat{H} Z^* a^* = Z^T \hat{H} W^* \quad (6.)$$

noting that  $\hat{H}^c = \hat{H}$ , since all of the values of  $\hat{H}$  are real. Recognizing that

$$(Z^T \hat{H} Z^*)_{j,k} = \langle Z'_j, Z'_k \rangle = \delta_{j,k},$$

where the notation  $X_{j,k}$  refers to the element of array  $X$  at position  $(j,k)$ ,  $Z^T \hat{H} Z^*$  is therefore the identity matrix. I then obtain the following solution for  $a$  from (6.) (after taking the conjugate of both sides),

$$a = Z^{*T} \hat{H} W.$$

So the new wind field  $Y$  expressed in terms of  $Z$  is

$$Y = Z a. \quad (6.)$$

Finally, in order to correct for any biases the analysis scheme may have introduced in  $Y$  and to preserve the amplitude of the COADS observations, the following procedure was used:

1.) The ratio of the average amplitude of the COADS anomalies to the analyzed anomalies is first formed as follows:

$$\chi = \frac{\sum_{s=1}^S W_s \wp_s}{\sum_{s=1}^S Y_s \wp_s}$$

where  $W_s$  represents the COADS observation at position  $s$ ,  $Y_s$  is the analyzed anomaly at position  $s$  yielded by (6.) and  $\wp_s$  is equal to 1 if there is a COADS observation at that position  $s$  or 0 otherwise.

2.) The analyzed anomalies are then scaled by  $\chi$ , i.e.,

$$\hat{Y} = \chi Y.$$

$\hat{Y}$  then constitutes the new pseudo-stress anomalies.

## 5. Model

A nonlinear reduced gravity model in spherical coordinates is used to simulate the variability in the equatorial Pacific due to wind stress forcing. This type of model has been used successfully in previous studies of tropical Pacific variability (e.g. Busalacchi and O'Brien, 1981; Kubota and O'Brien, 1988; Bigg and Inoue, 1992). The model consists of one dynamically active layer of a density  $\rho$  and depth  $h$  on top of an infinitely deep layer of slightly higher density  $\rho + \Delta\rho$ . The interface between these two layers is a proxy of the ocean pycnocline. Spherical coordinates are used due to the latitudinal extent of the model (20S-25N). The equations defining the model are,

$$\begin{aligned} \frac{\partial U}{\partial t} + \frac{1}{a \cos \theta} \frac{\partial}{\partial \varphi} \left( \frac{U^2}{h} \right) + \frac{1}{a} \frac{\partial}{\partial \theta} \left( \frac{UV}{h} \right) - (2\Omega \sin \theta) V \\ = -\frac{g'}{2a \cos \theta} \frac{\partial h^2}{\partial \varphi} + \frac{\tau_\varphi}{\rho} + A \nabla^2 U \end{aligned} \quad (1a)$$

$$\begin{aligned} \frac{\partial V}{\partial t} + \frac{1}{a \cos \theta} \frac{\partial}{\partial \varphi} \left( \frac{UV}{h} \right) + \frac{1}{a} \frac{\partial}{\partial \theta} \left( \frac{V^2}{h} \right) + (2\Omega \sin \theta) U \\ = -\frac{g'}{2a} \frac{\partial h^2}{\partial \theta} + \frac{\tau_\theta}{\rho} + A \nabla^2 V \end{aligned} \quad (1b)$$

$$\frac{\partial h}{\partial t} + \frac{1}{a \cos \theta} \left( \frac{\partial U}{\partial \varphi} + \frac{\partial}{\partial \theta} (V \cos \theta) \right) = 0 \quad (1c)$$

where  $\phi$  and  $\theta$  are the longitude and latitude, respectively;  $U$  and  $V$  are the transport in the east-west and north-south directions, respectively;  $H$  is the initial depth of the upper layer;  $g'=(\Delta\rho/\rho)g$  is the reduced gravity;  $A$  is a horizontal eddy viscosity coefficient;  $\tau=\rho_a C_D W|W|$  is the wind stress;  $\rho_a$  is the air density;  $C_D$  is a constant drag coefficient;  $W$  and  $|W|$  are the wind velocity vector and its magnitude, respectively;  $a$  is the radius of the earth; and  $\Omega$  is the angular velocity of rotation of the earth. The terms  $A\nabla^2 U$  and  $A\nabla^2 V$  parameterize the horizontal transfer of momentum by turbulent eddy processes. Model parameter values used are listed in Table 2.

Equations (1 a-c) were integrated over the domain 20S-25N and 124E-76W (see Figure 10). The equations were discretized using a staggered grid (Arakawa C-grid). The coastlines have no-slip and no normal flow boundary conditions imposed on them. The north and south boundaries are open, employing a numerically implemented Sommerfeld radiation condition (see Camerlengo and O'Brien, 1980).

A sample response picture, taken from the model solution for 25 March 1985 is shown in Figure 10. This model reproduces various climatological features of the equatorial Pacific: a thermocline which deepens from east to west, the North Equatorial Current, the North Equatorial Countercurrent, the South Equatorial Current, the subtropical gyre, the Kurishio and the equatorial cold tongue as well as several other features.

**Table 2.** The model parameters used. The zonal resolution is defined as the grid distance between adjacent u and h points and the meridional resolution is defined as the grid distance between adjacent h and v points.

model parameter	value
reduced gravity( $g'$ )	$.02 \text{ m s}^{-2}$
earth's rotation rate( $\Omega$ )	$7.292 \times 10^{-5} \text{ s}^{-1}$
initial depth( $H_{init}$ )	$200 \text{ m}$
air density( $\rho_{air}$ )	$1.2 \text{ kg m}^{-3}$
sea water density( $\rho_{water}$ )	$1025 \text{ kg m}^{-3}$
eddy viscosity( $A$ )	$750 \text{ m}^2 \text{ s}^{-1}$
drag coefficient( $C_D$ )	$1.5 \times 10^{-3}$
time step( $\Delta T$ )	$1800 \text{ s}$
zonal resolution( $\Delta\phi$ )	$1/8^\circ$
meridional resolution( $\Delta\theta$ )	$1/8^\circ$

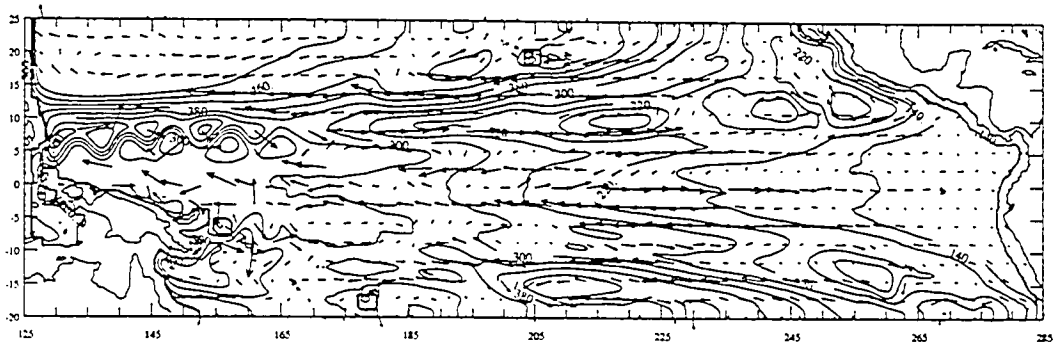


**Figure 10.** The domain of the oceanic model used ( $124^{\circ}\text{E}$ - $76^{\circ}\text{W}$ ,  $20^{\circ}\text{S}$ - $25^{\circ}\text{N}$ ). The picture corresponds to the model solution for 25 March 1985.



## 6. Results and Discussion

### 6.1. FSU EOF analysis

The percent variances for the first 40 modes from the FSU EOF analysis are shown in Table 3. The percent variances range from a high of 9.18% for mode 1 to 0.51% for mode 40. In an EOF analysis it is desirable to have a large portion of the variance accounted for by the first few eigenmodes, thereby increasing the likelihood that the most significant eigenmodes are physically meaningful. In this case the first three eigenmodes account for less than 24% of the variance and there aren't large differences in the variance accounted for between adjacent eigenmodes. Since it is difficult to distinguish physically the meaning of a given eigenmode in cases where the percent variances are close together, spatial patterns and time series will not be shown.

### 6.2. sample analysis month

In order to test the ability of this technique to reliably reconstruct complete pseudo-stress fields from sparse observed data, several months from the data rich period (post-1960) were subsampled to simulate months with poor data coverage. The analyzed pseudo-stress anomalies which corresponded to the original and subsampled observed fields were then checked for consistency.

**Table 3.** The percent variances accounted for by the first 40 eigenmodes yielded by the EOF decomposition of the FSU pseudo-stress product.

mode	percent variance	cumulative variance
1	9.18	9.18
2	7.41	16.59
3	6.98	23.58
4	4.45	28.02
5	3.66	31.69
6	3.43	35.12
7	3.25	38.36
8	2.76	41.13
9	2.46	43.58
10	2.28	45.87
11	2.11	47.98
12	1.94	49.92
13	1.77	51.69
14	1.64	53.32
15	1.42	54.75
16	1.36	56.11
17	1.33	57.44
18	1.23	58.67
19	1.18	59.84
20	1.07	60.92

mode	percent variance	cumulative variance
21	1.04	61.95
22	0.99	62.95
23	0.95	63.89
24	0.93	64.82
25	0.87	65.70
26	0.85	66.55
27	0.82	67.36
28	0.79	68.15
29	0.73	68.89
30	0.73	69.62
31	0.70	70.32
32	0.68	71.01
33	0.65	71.66
34	0.62	72.28
35	0.60	72.88
36	0.56	73.44
37	0.55	74.00
38	0.54	74.54
39	0.52	75.06
40	0.51	75.57

I chose to examine December 1962 as an example. In Figure 11(a.) the monthly mean COADS pseudo-stress anomalies (defined to be departures from the FSU pseudo-stress data set's monthly climatology) are shown. There were a total of 1545 positions in the domain of interest which had at least one observation. The monthly mean pseudo-stress anomalies for December 1962 were then subsampled to resemble the observation distribution for December 1934 (Figure 11(b.)). There were a total of 639 positions with at least one observation in the domain of interest.

The pseudo-stress anomalies yielded via the analysis for the original and subsampled observed fields for December 1962 are shown in Figures 12(a.) and (b.). The root mean square discrepancy between the COADS observations and analyzed values (Figure 11(a.) and 12(a.)) for this month is  $5.1 m^2 s^{-2}$ . The difference between the analyzed fields based on the original and subsampled observations is shown in Figure 12(c.). Note the regions of large differences coincide with areas where there were observations in 1962, but not in 1934. The large anomaly band south of the equator in Figure 12(a.) is significantly weakened and a spurious anomaly is created in the southeast corner of the domain.

The root mean square discrepancy for the period 1930-1989 is shown in Figure 13. The mean discrepancy for this period is  $5.62 m^2 s^{-2}$ . The discrepancy shows a downward trend throughout the period, coinciding with an increase in the quantity of observations. The upturn in the discrepancy during 1980-1989

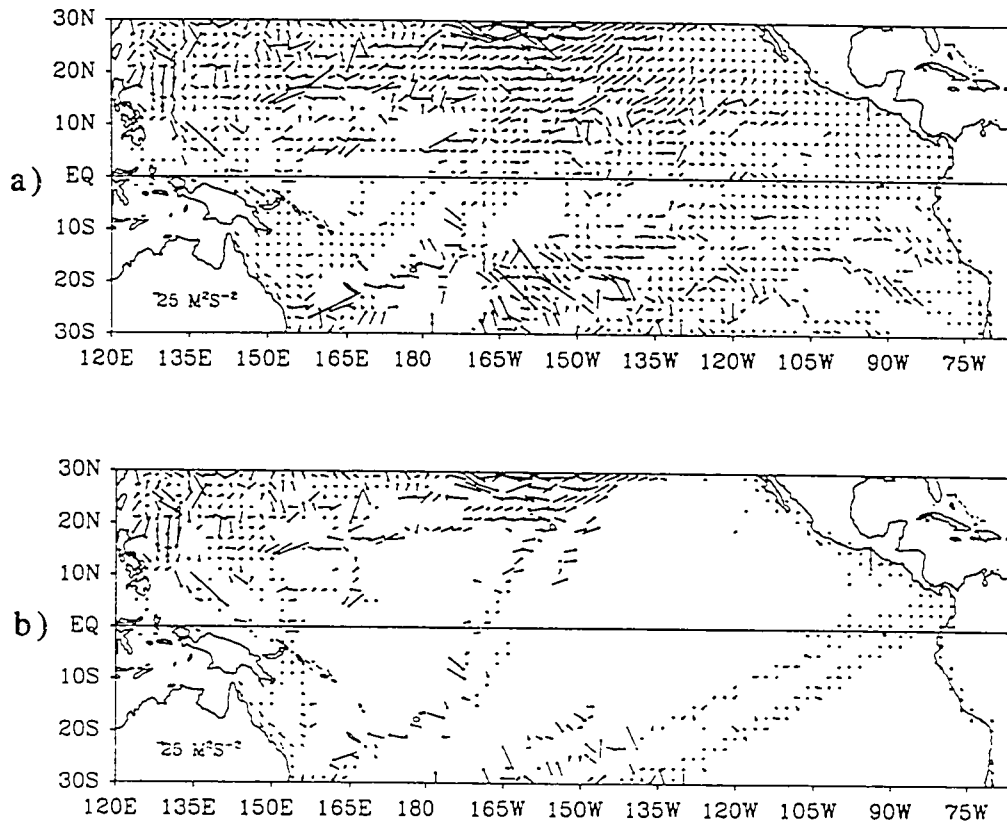


**Figure 11.** The (a.) COADS observations for December 1962 (610 missing values) and (b.) the COADS observations for the same month subsampled to resemble the observation distribution of December 1934 (1516 missing values).

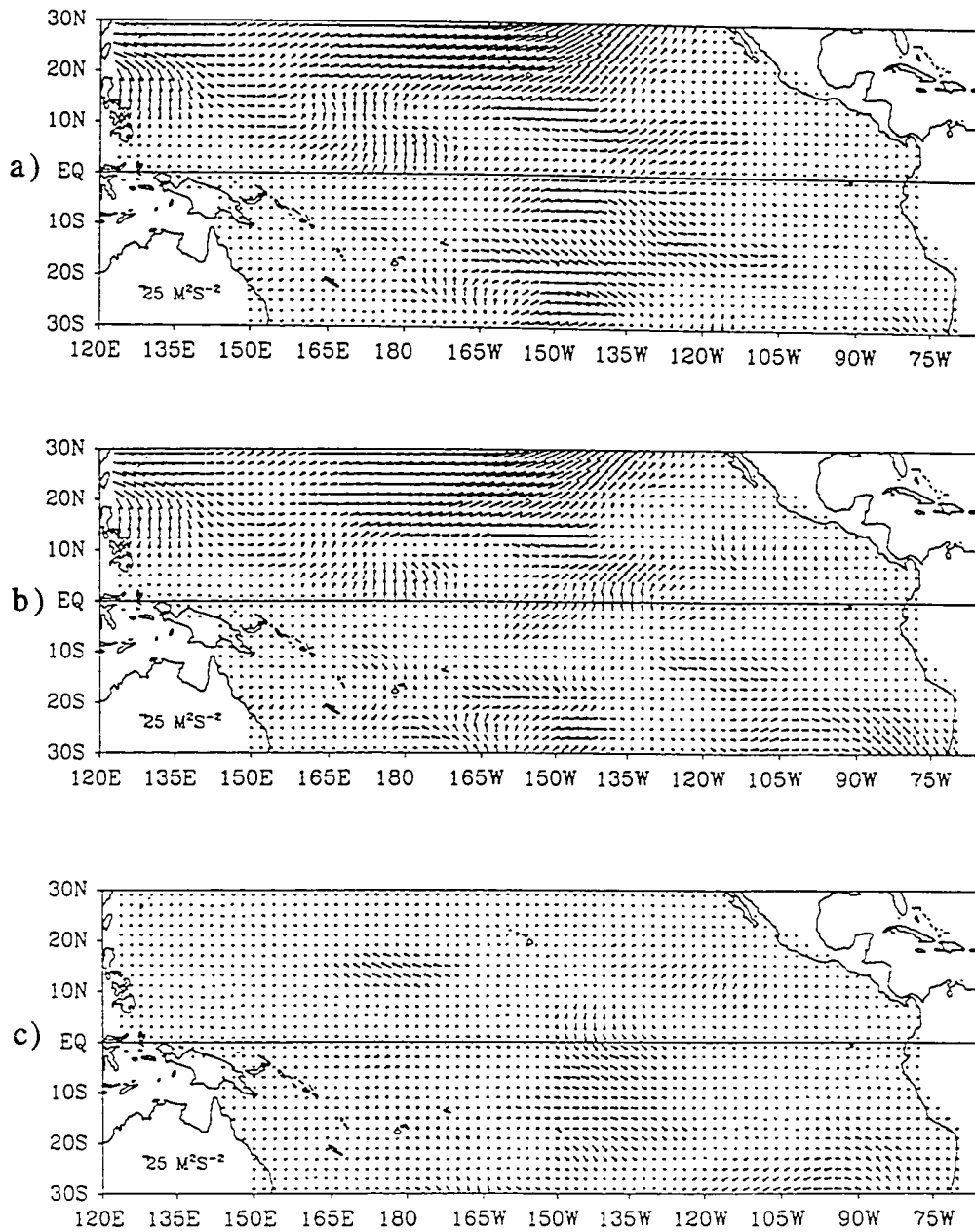


**Figure 12.** The analyzed anomaly fields corresponding to (a.) the COADS observations for December 1962 and (b.) the COADS observations for the same month subsampled to resemble the observation distribution of December 1934. The difference between the fields depicted in (a.) and (b.) is shown in (c.).

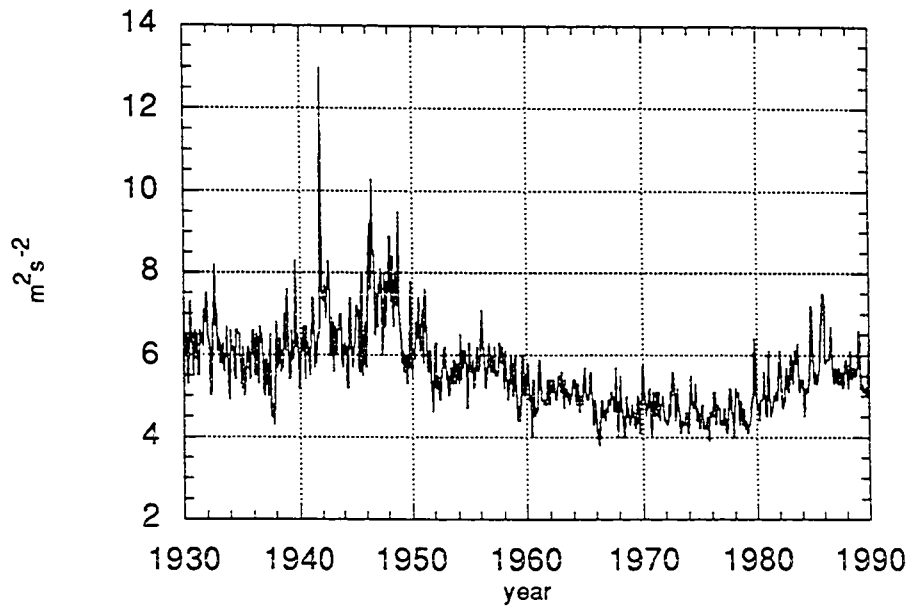


**Figure 13.** The root mean square discrepancy between the COADS observations and analyzed pseudo-stress anomalies for the period 1930-1989. the mean discrepancy is  $5.62 m^2 s^{-2}$ .

coincides with a period where the spatial availability of observations decreases by approximately 10%.

### 6.3. *detrending*

Several papers have been written examining trends in COADS pseudo-stresses (e.g., Ramage, 1987; Whysall *et al.*, 1987; Posmentier *et al.*, 1989 and Cardone *et al.*, 1990). There is no clear agreement, however, as to whether these trends are due to real climatic change or some other reason. Ramage (1987) identifies two trends in COADS pseudo-stresses; a decrease in amplitude prior to 1920 and an increase in amplitude since WWII. He attributes the first trend to the transition from sailing ships to steam, the second to changes in estimating procedure and the growing number of ships with anemometers. The new pseudo-stress data set is detrended according to Ramage's findings. The  $x$  and  $y$  slopes of the post WWII trend are equal to  $-4.67 \times 10^{-2} m^2 s^{-2}$  and  $3.50 \times 10^{-3} m^2 s^{-2}$  respectively. The  $x$  slope component is consistent with that documented in Posmentier *et al.* (1989).

### 6.4. *interannual variability*

It was demonstrated earlier (Section 6.2), using a sample analysis month, that the analysis produced anomalies which were consistent with the COADS observations. The next question to ask is how well did the analysis scheme used reconstruct the overall wind field. This validation was accomplished in two ways:

1.) The new wind fields were examined directly. The new wind product was then examined to see if it exhibited certain characteristics which have been shown to be important in terms of exciting El Niño events.

2.) The new pseudo-stress data set was then used to force an ocean model. Interannual fluctuations in ULT and currents were then examined and compared with observations.

In Section 6.4.1 I examine and validate the spatially averaged SST anomalies discussed in Chapter 2. Since this data set will be shown to be a good indicator of the magnitude and timing of El Niño events, it will be used as a validation data set in subsequent sections. In Section 6.4.2 the new pseudo-stress data set will be examined to see if it contains features which have been shown to be important in terms of exciting El Niño events. In Sections 6.4.3-6.4.4 fluctuations in ULT are investigated at several positions in the domain of interest. In Section 6.4.5 fluctuations in the North Equatorial Countercurrent are examined. In all cases, for validation purposes, model output is compared with either observed island sea level or spatially averaged SST anomalies.

#### 6.4.1. *average SST anomalies*

For validation purposes, a data set which reliably indicated low frequency fluctuations in the eastern Pacific for the period



1930-1989 was necessary. The data set which I chose to use was the spatially averaged SST anomalies discussed in Chapter 2 (see Figure 5). The number of positions where there was at least one SST observation in the area  $150^{\circ}\text{W}$ - $90^{\circ}\text{W}$ ,  $4^{\circ}\text{S}$ - $4^{\circ}\text{N}$  as a function of time is shown in Figure 14. The total number of positions ranges from 60-80 for the period 1960-1990, but tails off to less than 40 by 1950. There are several months where there were no observations, and these months are filled using linear interpolation. The low number of spatial positions with at least one observation, in particular, before 1950, raises the question of how reliable the average SST anomalies are as a data set to validate occurrences of El Niño.

The way I chose to validate the El Niño events indicated in the SST anomalies was as follows:

- 1.) Use the JMA El Niño definition to identify years in which there were El Niño events.
- 2.) Compare the El Niño events indicated by the SST anomalies with those documented in Quinn *et al.* (1987).

The El Niño events obtained via the spatially averaged SST anomalies for the period 1930-1989 are listed in Table 4. The El Niño events as documented in Quinn *et al.* (1987) are listed in Table 1. Comparison of the two tables shows that the SST

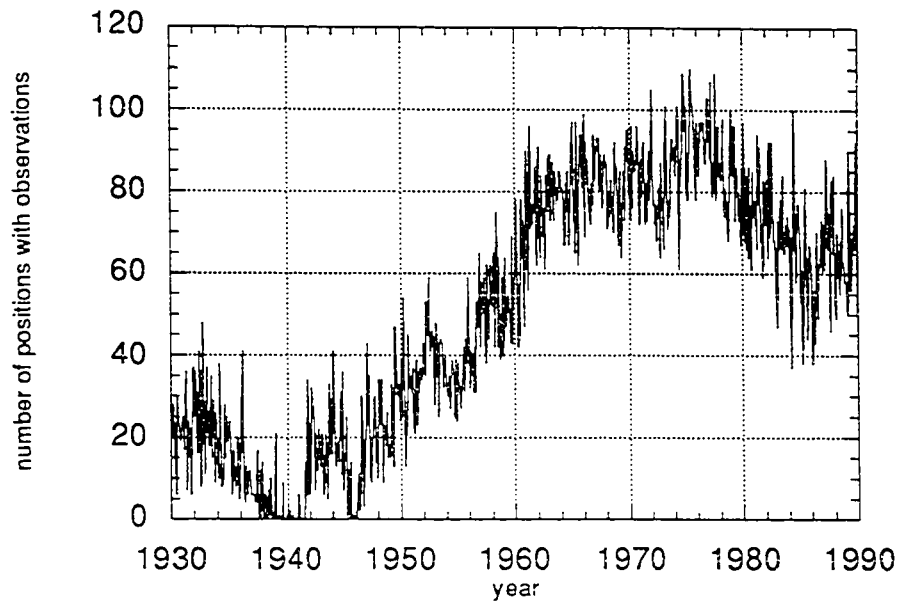


**Figure 14.** The number of positions in the area  $150^{\circ}\text{W} - 90^{\circ}\text{W}$  and  $4^{\circ}\text{N} - 4^{\circ}\text{S}$  where there was at least 1 observation.

**Table 4.** Years of El Niño events using the Japan Meteorological Agency criteria.

El Niño years
1931
1936 - 37
1939 - 40
1943
1951
1957 - 58
1963
1965
1969
1972 - 73
1976
1979
1982 - 83
1986 - 87

anomalies contain all the Quinn *et al.* El Niño events with the exception of 1932 and 1953. Inspection of Figure 5, however, reveals that there was anomalous warming in the eastern equatorial Pacific in 1932 and 1953, but they weren't of sufficient duration and amplitude to satisfy the JMA El Niño criteria.

It was necessary to process each time series identically for consistency in order to compare the average SST anomalies with other time series. Since all the time series examined in this section have their post-1965 climatology removed and a 12-month moving average applied to highlight the interannual variability, the average SST anomalies were processed similarly for use in subsequent sections.

#### 6.4.2. EOF analysis of new pseudo-stress data set

A first approach to validating that the new pseudo-stress data set contains sufficient physics to excite an El Niño response consistent with observations is to examine the pseudo-stress data set directly. Through numerical simulations (e.g. Busalacchi and O'Brien, 1981; Busalacchi *et al.* 1983; Cane, 1984) it has been shown that the most important aspect of the equatorial Pacific wind field in terms of exciting El Niño events is the zonal component in the west central part of the basin close to the equator. If an El Niño mode could be isolated within the new pseudo-stress data set I should expect to see a large spatial contribution somewhere near the dateline and El Niño-type variations in time. An EOF analysis was performed on the zonal

pseudo-stress anomaly along the equator averaged between 5°N and 5°S.

The first mode accounts for 41.29% of the variance. The spatial pattern (Figure 15) shows a large positive contribution centered near the dateline, with an area of negative contribution in the far eastern basin. The time series which modulates Figure 15 shows oscillations which are consistent with those in the average SST anomalies (see Figure 16). The correlation coefficient value for the 1st mode time series and the average SST anomalies is .71. The peaks in the first mode time series correspond to an increase in the zonal anomaly in the western basin, which would then result in a relaxation or reversal of the zonal component of the trades. This connection between the periods where the trades relax or reverse and the warm SSTs is exactly the El Niño mechanism put forth by Wyrtki. It can then be concluded that there is a significant El Niño mode within the new data set which has features consistent with those theoretical and numerical simulations would suggest I should expect to see.

#### 6.4.3. *sea level comparisons*

The next approach used to validate the new pseudo-stress data set was to use it to force an ocean model and then compare the model results with observations. A traditional data set used in the validation of a reduced-gravity model is observed sea level (eg. Busalacchi and O'Brien, 1981; Busalacchi and Cane, 1985; Kubota and O'Brien, 1988). Examination of the sea level data

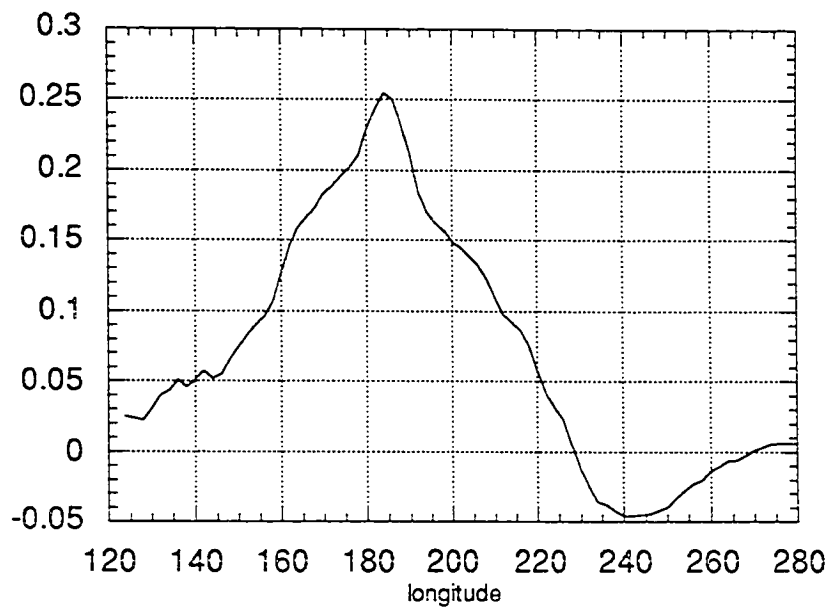


**Figure 15.** The first eigenmode's spatial pattern obtained from the EOF decomposition of the new pseudo-stress product. The first mode accounts for 41.29% of the variance.

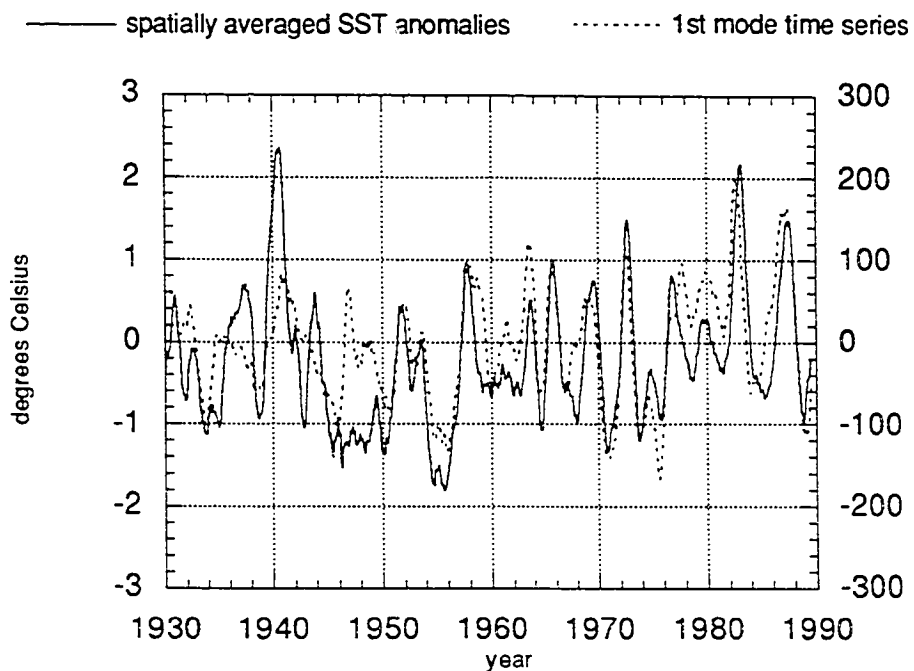


**Figure 16.** The time series which modulates the first eigenmode's spatial pattern. The average SST anomalies are plotted for comparison.

available in the PSMSL data set shows that the equatorial Pacific is extremely lacking in observed sea level data prior to about 1960. The lack of observed sea level prior to 1960 therefore prevents a thorough validation in space and time.

I chose to examine interannual fluctuations in the oceanic response near the equator by considering two locations on opposite ends of the equatorial Pacific basin. The two locations used are Galapagos and Truk. The locations of Galapagos and Truk are shown in Figure 2.

Model sea level anomalies at a location corresponding to Galapagos are shown in Figure 17. The model sea level anomalies were formed by multiplying the model ULT anomalies by  $\frac{\Delta\rho}{\rho}$ . The model sea level fluctuations and observed sea level (plotted for comparison) have had their monthly means (post-1965) removed and then were filtered using a 12-month running mean to highlight the interannual variability. The model clearly identifies El Niño events (positive anomalies) in 1963, 1965, 1969, 1972, 1976, 1982 and 1986. The timing and relative amplitudes of these events are consistent with the El Niño occurrences and strengths documented by Quinn *et al.* (1987) in Table 1. The fluctuations in model sea level compare well with those in the observed Galapagos sea level anomalies ( $r=.73$ ). The model sea level data exhibits a "climatic shift" in the mid 1970's which is not present in the observed sea level data. This climatic shift that the model sea level indicates was also observed in North Pacific sea level



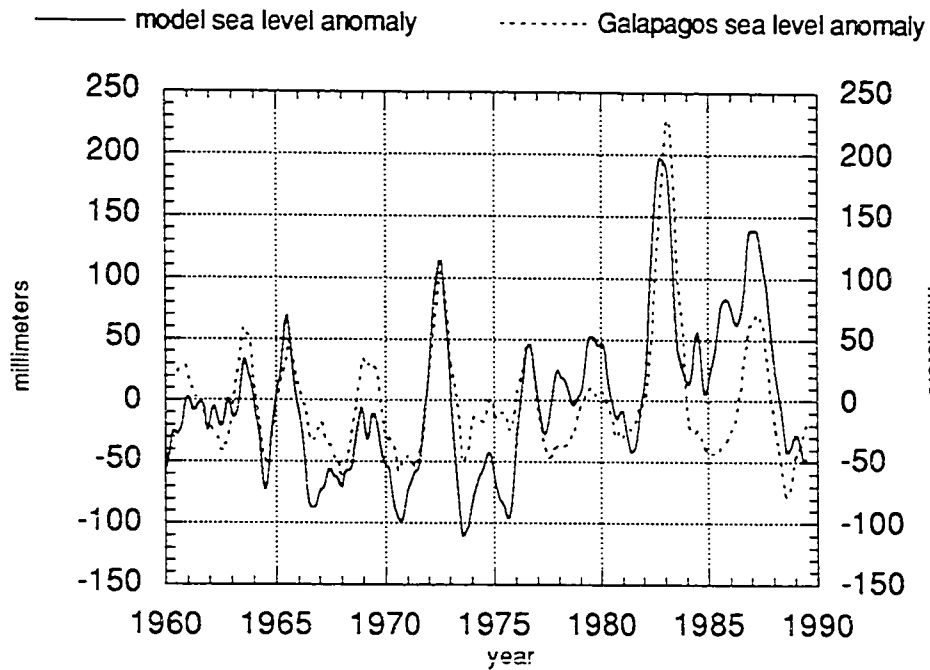


**Figure 17.** The model sea level anomalies at a location corresponding to Galapagos and observed Galapagos sea level anomalies. The model sea level anomalies were formed by multiplying the model ULT anomalies by  $\frac{\Delta\rho}{\rho}$ .

pressure and 500 mb heights (Oceanic Interdecadal Climate Variability, *IOC Technical Series 40*. UNESCO, 1992). Note also that the cold events (negative anomalies) are also resolved well in terms of amplitude and timing.

Model sea level fluctuations at a location corresponding to Truk are shown in Figure 18. The model sea level fluctuations and observed sea level (plotted for comparison) have had their monthly means (post-1965) removed and then were filtered using a 12-month running mean to highlight the interannual variability. The y axes in Figure 18 have been reversed so that peaks in the curve correspond to El Niño years. Model sea level falls corresponding to the El Niño events of 1957-58, 1963, 1965, 1969, 1972, 1976 and 1982-1983 are evident. The model reproduces the observed sea level fluctuations at Truk well, with the exception of some phase disagreement around 1967 and missing the positive sea level anomaly around 1962. The correlation coefficient for these two time series is .71.

#### *6.4.4. comparisons with average SST anomalies*

I next examined model ULT anomalies averaged over the area 4°N-4°S and 150°W-90°W (see Figure 19). Comparison of the model ULT time series with the spatially averaged SST anomalies (plotted for comparison) demonstrates that the model resolved the warm events (positive anomalies) and the cold events (negative anomalies) well, with the exception of the period 1945-1949. The disagreement in the period 1945-49 can be explained

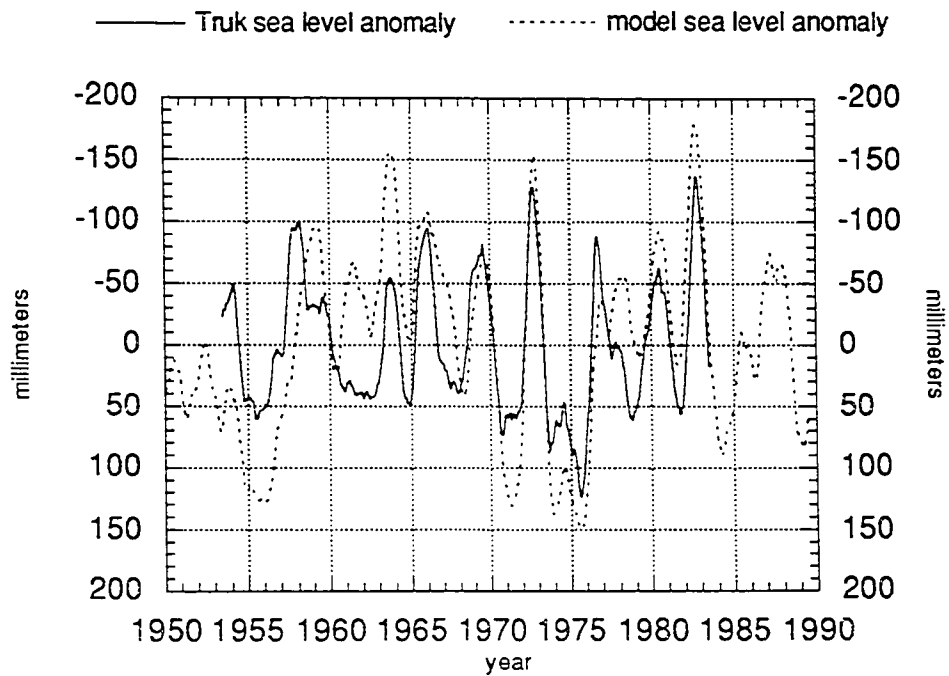


**Figure 18.** The model upper layer thickness data at a location corresponding to Truk and observed Truk sea level.

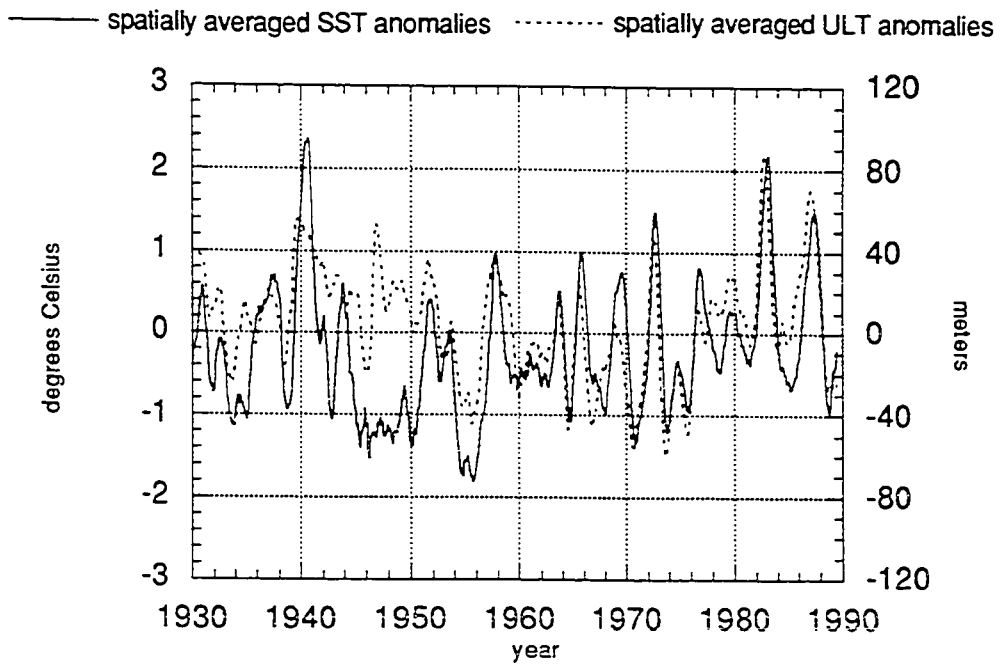


Figure 19. The SST and ULT anomalies averaged over the area 150°W - 90°W, 4°N - 4°S.

by the following. As discussed in Section 6.4.2, the region of largest influence for forcing eastern equatorial Pacific sea level variations is found close to the equator in the area around the dateline. Looking at the observation distributions shown in Chapter 3 note the good density of observations in the vicinity of the dateline for the period 1940-44 (Figure 6(c.)) and 1950-54 (Figure 7(b.)), but there are almost no observations along the equator for the five year period 1945-49 (Figure 7(a.)). The disagreement during the 1945-1949 period can then be attributed to extremely poor data coverage in the west central basin during this period. The data coverage during this period was so poor in the region of largest influence that the analysis scheme wasn't able to produce pseudo-stress fields which contained the necessary physics to excite eastern Pacific variability which was consistent with observations.

A feature of note in Figure 19 is the climate shift of the mid 1970's. This climatic shift was previously noted in North Pacific sea level pressure and 500 mb heights and eastern Pacific model sea level anomalies. The climate shift of the mid 1970's is clearly evident in the averaged SST and ULT anomalies depicted in Figure 19. The correlation coefficient of the two time series is .63.

#### 6.4.5. *North Equatorial Countercurrent*

The North Equatorial Countercurrent (NECC), an eastward flowing current between the westward flowing North and South Equatorial Currents, owes its existence to variations in the trades

from north to south across the equator. In the model simulation, the NECC shows significant variability about its mean position of approximately  $6^{\circ}\text{N}$  (see Figure 20). This type of meridional variability in the position of the NECC is consistent with observations. In order to make a single time series to examine fluctuations in the modeled NECC, the zonal velocity component at this longitude is averaged between  $3^{\circ}\text{N}$  and  $12^{\circ}\text{N}$ .

Interannual fluctuations in the modeled NECC for 1950-1989 are shown in Figure 21. The monthly climatology (1966-89) has been removed and a 12-month moving average has been applied to highlight the interannual variability. There are several interesting features evident in this figure. The two curves have a correlation value of  $r=.70$  with the NECC anomalies lagging the SST anomalies by 5-months. The NECC shows a strengthening during El Niño events, where the relative magnitudes of the NECC fluctuations are indicative of the strength of the event. The enhanced NECC acts to transport warm water eastward during an El Niño event and it relaxes during cold events. Wyrтки (1974) inferred variations in the strength of the NECC by considering observed sea level differences across the current (Figure 22). The modeled NECC shows fluctuations that are consistent, in terms of amplitude and timing, with the results of Wyrтки.

#### 6.4.6. *comparisons with FSU forced response*

When the new pseudo-stress data set was formed, the statistically significant spatial patterns (which accounted for 75%

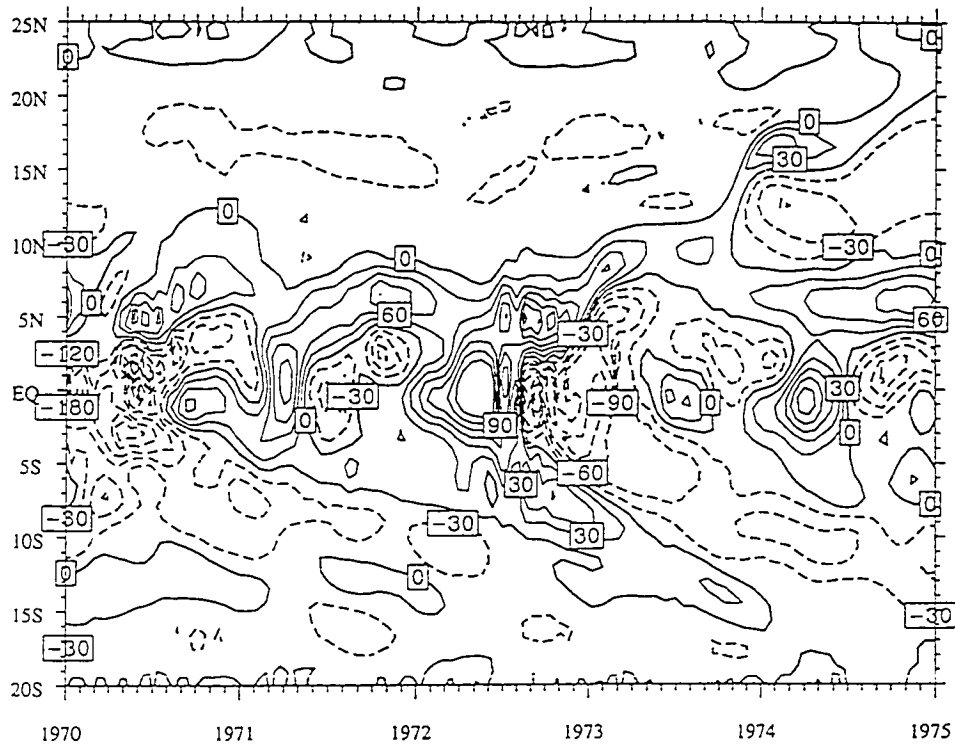


**Figure 20.** Contours of zonal velocity at  $140^{\circ}\text{W}$ . The solid lines denote eastward velocities. Note the considerable variability in the position of the North Equatorial Countercurrent (mean position of approximately  $6^{\circ}\text{N}$ ).

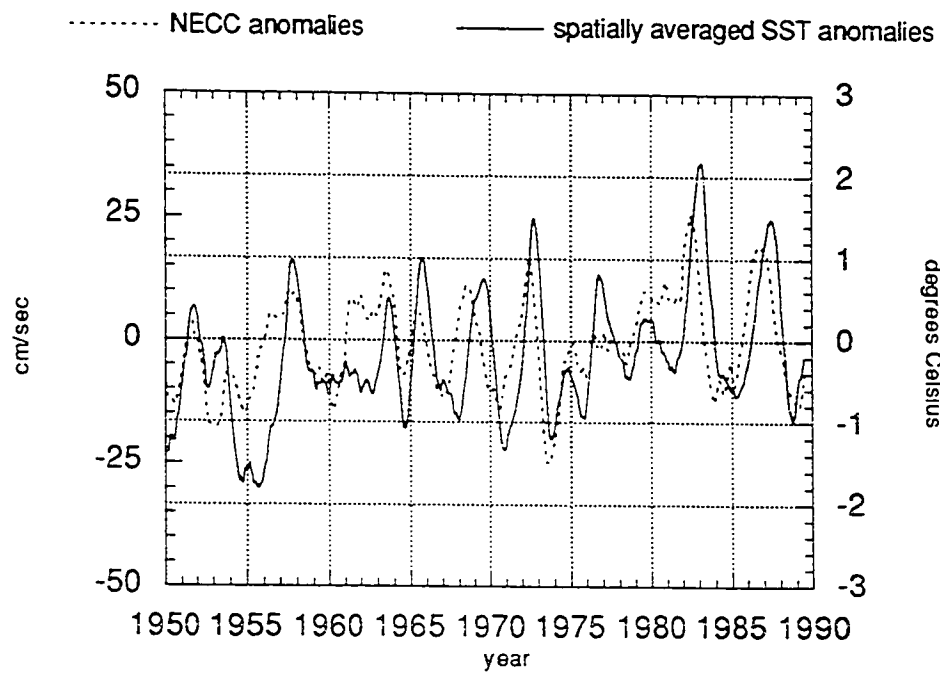


**Figure 21.** Interannual fluctuations in the model North Equatorial Countercurrent. The values plotted are obtained by averaging the  $x$  velocity at  $140^{\circ}\text{W}$  between  $3^{\circ}\text{N}$  and  $12^{\circ}\text{N}$ . The average SST anomalies are plotted for comparison.



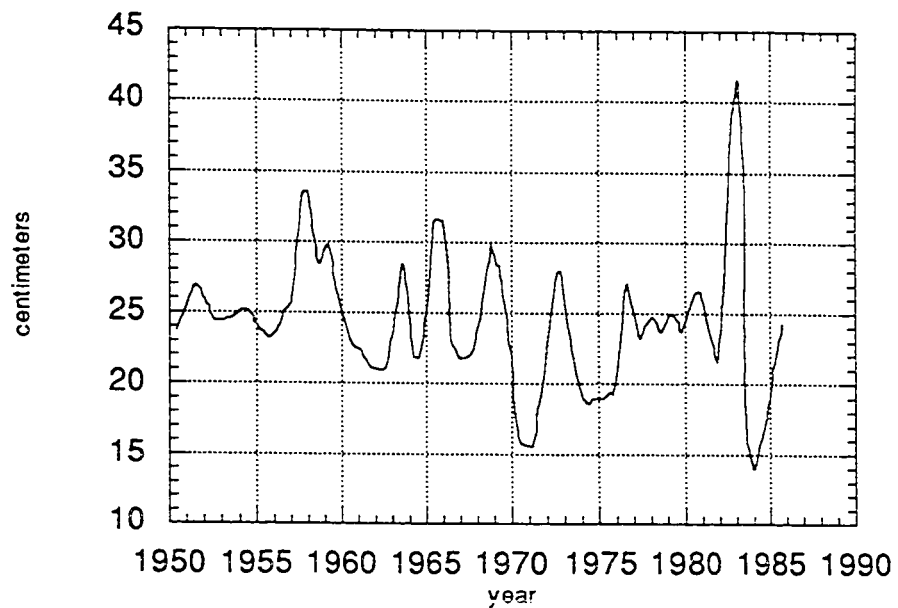


**Figure 22.** Time series of sea level differences across the North Equatorial Countercurrent in the central Pacific for the period 1950-1985 (from Wyrтки (1974), who later extended the time series to 1985).

of the variance) from the FSU data set were used as the climate basis functions for the new data set. By not considering the non-statistically significant spatial patterns in the analysis approximately 25% of the variance which can encompass both physics and noise was omitted. It is then reasonable to ask what difference does the omission of the non-statistically significant modes make in terms of the new data set's ability to excite interannual fluctuations in the equatorial Pacific consistent with observations? To answer this question a separate model run was performed where the FSU pseudo-stress data set was used as the forcing.

The model ULT response compared with observed sea level from Galapagos is shown in Figure 23. The model generally does a good job replicating the observed interannual fluctuations. The model, however, overestimated the warm event in 1965 and generally overestimated the cold events. The correlation coefficient for these two time series is .71.

The model sea level - Galapagos sea level comparison for the case where the new pseudo-stress data set is used as the forcing is shown in Figure 17. Calculations show that the results obtained using the two different forcings account for approximately the same amount of variance (approximately 50%). However, the case where the new wind fields are used as the forcing appears to produce a response which generally does a better job of replicating the observed fluctuations. The factor accounting for the difference is the following. Posmentier *et al.* (1989)

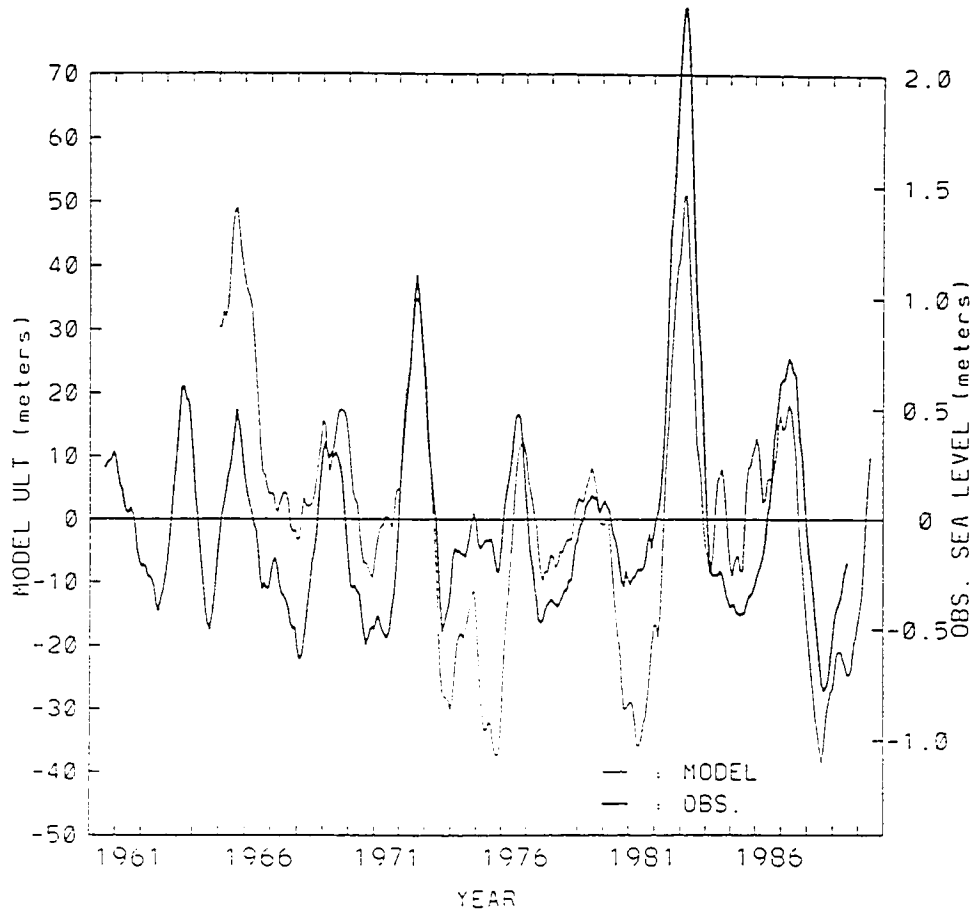


**Figure 23.** The anomalous ULT fluctuations at a location corresponding to Galapagos vs. observed sea level anomalies. The model forcing in this case is the FSU pseudo-stress data set.

documents a trend in the zonal stress in the eastern equatorial Pacific in the FSU data set of  $-2.81 \times 10^{-2} m^2 s^{-2} month^{-1}$ , representing a strengthening of the prevailing easterly trades. Such a strengthening of the trades would produce a corresponding decrease in eastern equatorial Pacific ULT, as seen in Figure 23. Such a trend in ULT is not seen in Figure 17 because the new pseudo-stress data set was detrended prior to forcing the model.

### 6.5. *interdecadal variability*

In the previous section I examined interannual variability in the new pseudo-stress data set, model ULT and the NECC. It was shown that

- 1.) The new data set contained a significant El Niño mode which had features consistent with theory and observations.
- 2.) Using the new data set to force the ocean model, it was found that the model response was consistent with observations.

In this section interdecadal variability will be examined in global mean land air temperature, spatially averaged model ULT and observed SST anomalies.

#### 6.5.1. *global mean land air temperature*

In Figure 24 a plot of global mean land air temperature is shown. The first feature of note is the upward trend which persists throughout the 20th century. There is also considerable

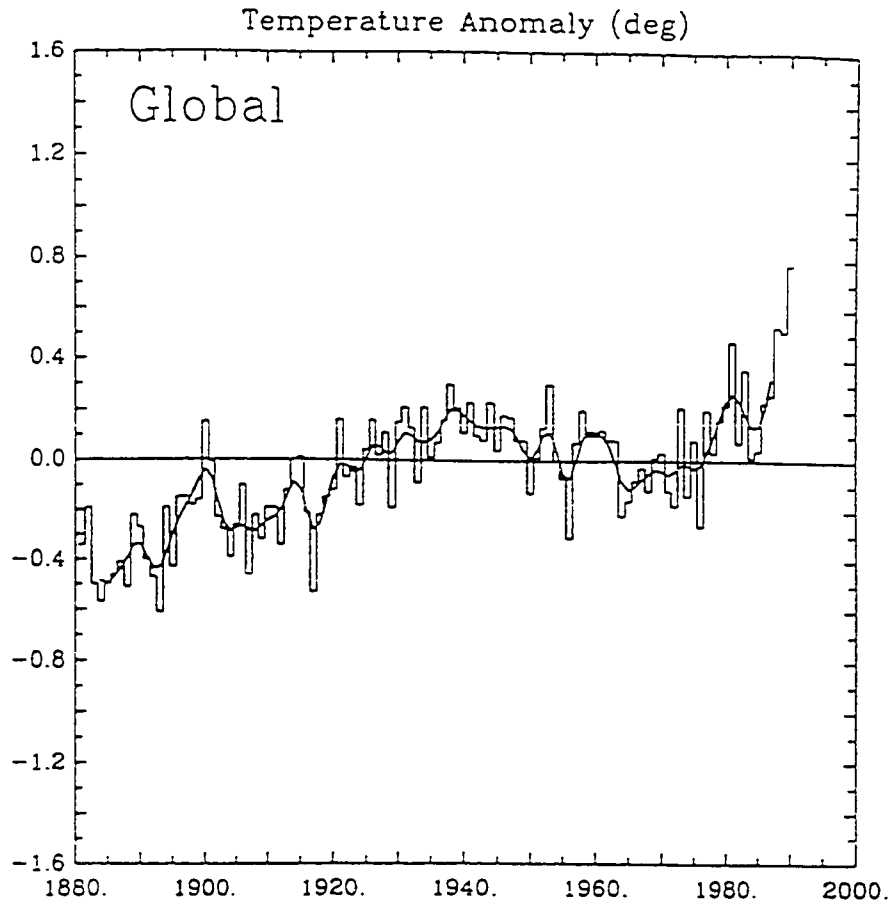


**Figure 24.** Global mean land air temperature anomalies relative to 1951-1980 (Annual values and smoothed curves) (from *Oceanic Interdecadal Climate Variability, IOC Technical Series 40*. UNESCO, 1992).

interannual and interdecadal variability superposed upon this upward trend. Focusing upon my period of interest, 1930-1989, there are warm peaks around 1940, 1960 and 1980. There is also a prolonged cooling connecting the peaks in 1960 and 1980. The climatic shift of the mid 1970's which has been noted in the north and equatorial Pacific, is also evident in the global mean land air temperature.

#### 6.5.2. *Eastern Pacific*

A Butterworth filter was applied to the average ULT and SST data in Figure 19, allowing examination of interdecadal variability in eastern equatorial Pacific ULT and SST. The filtered curves are shown in Figure 25. The low passed model ULT exhibits several very interesting features. The model ULT anomalies and the SST anomalies show good qualitative agreement. There are positive anomalies peaks in 1940, 1958 and 1982, with a prolonged negative anomaly connecting the peaks in 1958 and 1982. There is also a peak around 1950, but this spurious peak is the result of the model result missing the cooling which happened in this period (as discussed in 6.4.4). The warming in the eastern equatorial Pacific is not necessarily indicative of warming of the Pacific Ocean as a whole. For example, while the eastern equatorial Pacific was anomalously warm in 1982, Figure 26 shows that there was anomalous cooling in the North Pacific.

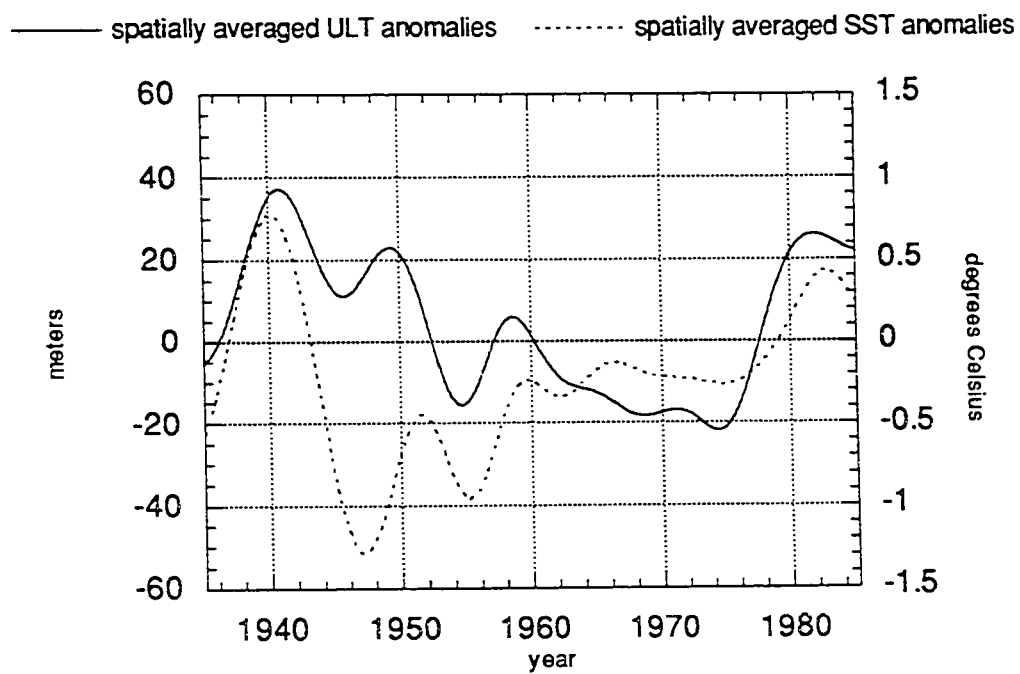


**Figure 25.** Low passed ULT and SST anomalies averaged over the area  $150^{\circ}\text{W} - 90^{\circ}\text{W}$ ,  $4^{\circ}\text{N} - 4^{\circ}\text{S}$ . To filter periods less than 10-years, a Butterworth filter was used.

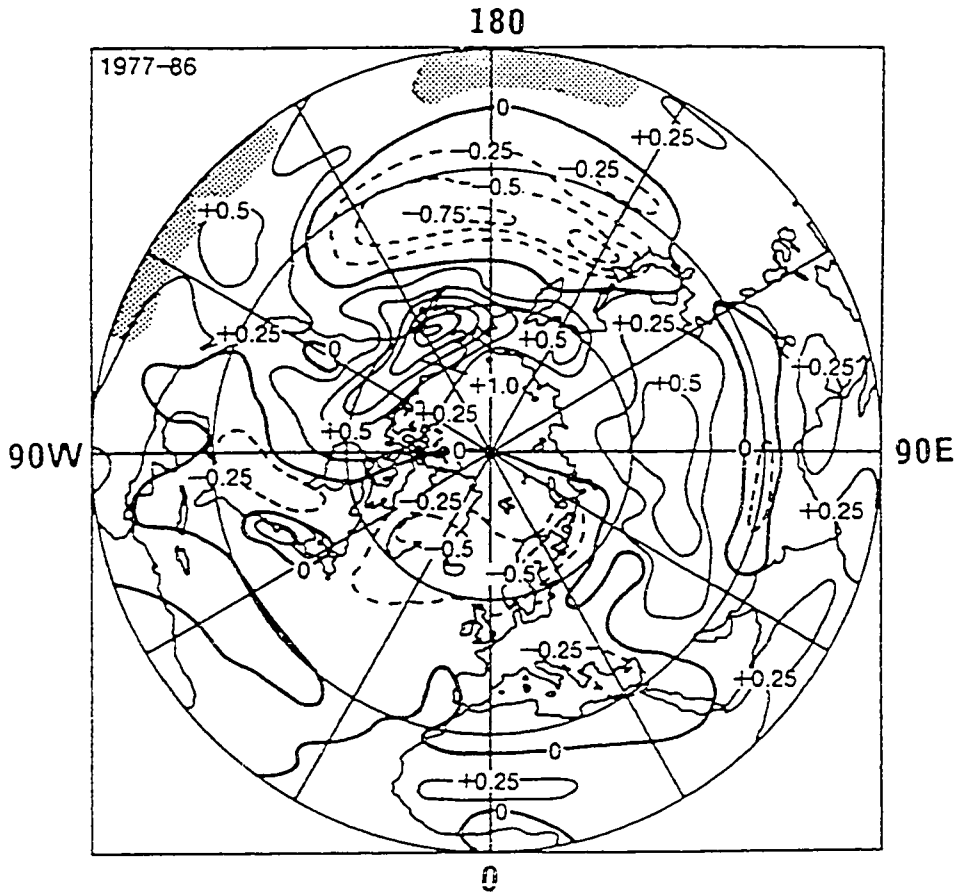


**Figure 26.** Decadal average air-surface temperature or sea surface temperatures as departures from the 1951-80 mean, for 1977-86 (from Trenberth, 1990).



The good qualitative agreement between Figures 24 and 25 would suggest that there is a connection between interdecadal fluctuations in eastern Pacific ULT and global mean land air temperature. A connection between El Niño warming in the tropical Pacific and global mean land temperature has been previously demonstrated (see Figure 27). The results in this study would suggest that this connection is also valid for interdecadal time scales, not just for El Niño period band (approximately 2-5 years).

The interdecadal fluctuations in eastern Pacific ULT serve another important purpose, modulating the amplitude of El Niño events. The large positive peak near 1940 corresponds to the anomalously warm climate in the tropical Pacific during the late 1930's and early 1940's. This was a highly active period, with 3 El Niño events happening in this time period (as documented by Quinn *et al.*, 1987). The positive peaks in the late 1950's and early 1980's coincide with the severe El Niño events of 1957-1958 and 1982-1983, respectively.

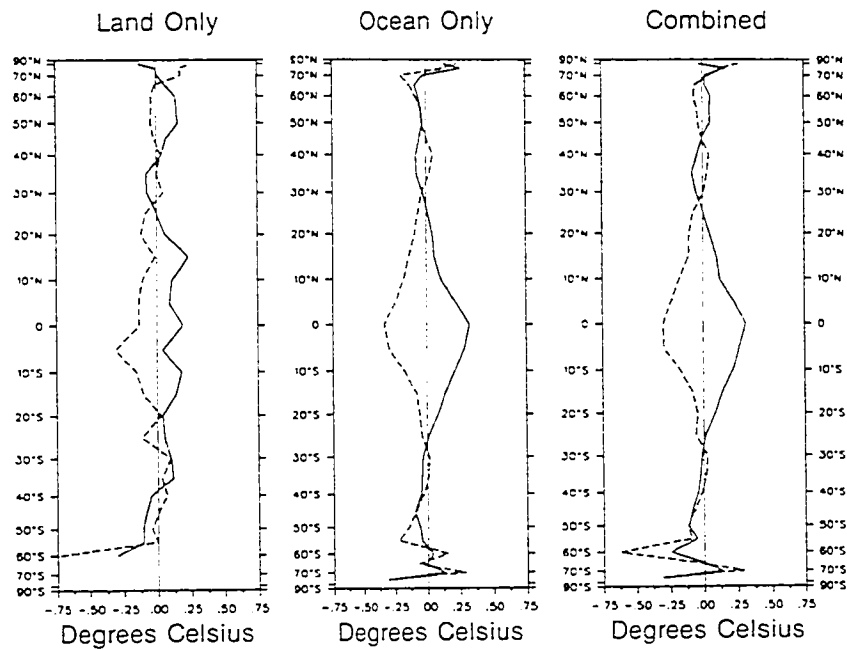


Figure 27. Profile of zonally averaged temperature anomalies ( $^{\circ}\text{C}$ ) over both land and ocean areas during El Niño (solid line) and El Viejo (dashed line). The events composited span the period 1887-1988, using a classification criteria described in Kiladis and Diaz (1989).

## 7. Summary and Conclusions

Poor data coverage over the world's oceans has greatly limited the period over which wind forced ocean models can be used in climate studies. Due to intense interest recently in low frequency climatic variability, a question arises: how far back in time can equatorial Pacific wind fields be compiled, suitable for model forcing, whereby accurate simulations of the equatorial Pacific can be carried out? Previous modeling efforts have focused on the relatively data rich period from 1960's to the present (e.g. Busalacchi and O'Brien, 1981; Cane *et al.*, 1986; Kubota and O'Brien, 1988). During this period, wind analyses produced at Florida State University have been shown to excite equatorial Pacific Ocean variability consistent with observations. In this research a new pseudo-stress data set spanning the period 1930-1989 was formed, effectively doubling the current period (1966-present) over which wind forced oceanic variability can be examined.

The new pseudo-stress data set was derived from observed COADS pseudo-stresses. The COADS data has 70-80% coverage from 1960-1990, but decreases to less than 20% by the turn of the century (see Figure 2). The sparse COADS coverage, particularly before 1960, necessitated an objective analysis scheme which incorporated physical constraints to overcome the analysis problems that very sparse data coverage poses.

Dominant spatial patterns for the period 1966-1990 were determined through an EOF analysis of the FSU subjectively analyzed wind stress product. It was then assumed that these dominant spatial patterns (termed climate basis functions) were representative of the spatial variability of the equatorial Pacific wind field for the period of interest (1930-1989). Using the climate basis function set, a variation of Cressman's (1959) objective analysis scheme and a technique called Vector Group Renormalization, monthly mean pseudo-stress maps are obtained for the period of interest (1930-1989).

After compiling the new data set, the next step was to determine how well the analysis scheme reconstructed the overall wind field. This question was answered in two ways: direct examination of the new wind fields and using them to force an ocean model. In both cases, observed data, sea level and spatially averaged SST anomalies, were used for comparison purposes.

Direct examination of the new data set was done via an EOF analysis. The first mode was found to account for 41.29% of the variance. The spatial pattern for this mode showed a large contribution centered near the dateline. The time series which modulates the first mode spatial pattern displayed variability which was consistent with that exhibited by the spatially averaged SST anomalies. It was concluded that this mode was an El Niño mode, possessing features consistent with those which theory and numerical simulations would suggest we should expect to see.

A shallow water, reduced gravity, nonlinear model was then forced with this new wind data set and the model response was compared with observations. Observed sea level at Galapagos and Truk were compared with model sea level values corresponding to the same locations, yielding correlation ( $r$ ) values of .73 and .71, respectively. To validate the eastern Pacific response, model ULT anomalies and observed SST anomalies averaged over the area  $4^{\circ}\text{N} - 4^{\circ}\text{S}$ ,  $150^{\circ}\text{W} - 90^{\circ}\text{W}$  were compared, yielding a correlation coefficient ( $r$ ) value of .63. The period of 1945-49, however, yields poor agreement.

The disagreement during the 1945-1949 period can be attributed to extremely poor data coverage in the west central basin during this period. The data coverage was so poor in the region of largest influence during this period that the analysis scheme wasn't able to produce pseudo-stress fields which contained the necessary physics to excite eastern Pacific variability which was consistent with observations.

Next, interdecadal variability in eastern Pacific ULT and SST were examined. The low frequency fluctuations in the ULT and SST data showed good qualitative agreement. Examination of global mean land air temperature showed low frequency fluctuations which were consistent with those in the ULT data. It has been previously demonstrated that there was a clear relationship between El Niño warming in the eastern Pacific and an increase in global mean land air temperature. My results

suggest that the connection between eastern Pacific Ocean and global mean land air temperature warming also holds for interdecadal time scales.

The interdecadal fluctuations in eastern Pacific ULT are shown to serve another important purpose, modulating the amplitude of El Niño events. The peaks in low-passed eastern Pacific ULT and SST in 1940, late 1950's and early 1980's correspond to the strong El Niño events of the late 1930's and early 1940's, 1957-1958 and 1982-1983.

## Appendix A

### *vector empirical orthogonal function analysis*

Vector Empirical Orthogonal Function (EOF) analysis is used on a  $m \times n$  matrix  $U$  to decompose it into its component eigenmodes, each accounting for a certain percentage of the original variance in  $U$ . The dimensions  $m$  and  $n$  can represent various physical quantities, such as height, spatial position and time. For illustrative purposes, let  $m$  and  $n$  represent space and time, respectively. The more significant eigenmodes may have physical interpretations associated with them.

The covariance matrix of  $U$  is given by

$$C = \frac{1}{m} U^* U$$

where  $*$ T denotes conjugate transpose.  $C$  is a Hermitian  $n \times n$  matrix having real eigenvalues.

The eigenvector decomposition of  $C$  yields  $n$  real eigenvalues  $\lambda_i$  and  $n$  associated complex eigenvectors  $E_i$  of length  $n$ . This set of  $n$  eigenvectors form an orthonormal basis from which the original data set  $U$  can be reconstructed.

Through vector EOF analysis a time by space data set can be represented as the product of a time vector (in this case  $E_i$ ) and a

spatial vector (in this case  $W_i$ ) summed over the total number of eigenmodes ( $n$ ), i.e.

$$U = \sum_{i=1}^n W_i E_i, \quad (1.)$$

where  $W_i$  is a vector of length  $m$ . To solve for  $W_i$  for a given  $i$  (eigenmode) right multiply both sides of (1.) by  $E_k^{*T}$ , yielding

$$W_k = U E_k^{*T}.$$

Through this technique,  $U$  has been decomposed into its component eigenmodes, each of which account for a certain percentage of the variance in  $U$ , given by

$$[\text{variance explained by eigenmode } i] = \frac{\lambda_i}{\sum_{k=1}^n \lambda_k}.$$



## Appendix B

### *test for mode significance*

A statistical test (Overland and Preisendorfer, 1982) was used to determine the statistically significant eigenmodes. An outline of how the procedure was implemented follows.

Let the normalized eigenvalues from the EOF decomposition of the FSU stress product be represented as

$$T_j = \frac{d_j}{\sum_{j=1}^N d_j}$$

where  $d_j$  represents the eigenvalue corresponding to eigenmode  $j$ .

Next a series of 20 random matrices identical in size to the FSU data set were formed, then an EOF analysis was performed, yielding the normalized eigenvalues

$$U_j^r = \frac{\delta_j^r}{\sum_{j=1}^N \delta_j^r}$$

where  $r$  corresponds to the trial (1,2,...,20) and  $\delta_j^r$  is the eigenvalue corresponding to trial  $r$  and mode  $j$ . The  $U_j^r$  values are then ordered so that  $U_1^r \leq U_2^r \leq \dots \leq U_N^r$ .

The number of statistically significant eigenmodes was then identified by comparing  $U_j^{19}$  with  $T_j$ . The choice of  $U_j^{19}$  is analogous to using 95% confidence limits. The maximum value of  $j$  where  $U_j^{19}$  is exceeded by  $T_j$  is then determined to be the number of statistically significant eigenmodes.

## Appendix C

### *t-test for validity of climatology*

The assumption that the FSU climatology was the correct climatology was validated via a t-test. The procedure used is outlined in the following.

I let  $C_{s,m,y}$  represent the COADS data which was demeaned using the FSU climatology, where  $s$  represents space (1,2,...,2155),  $m$  represents the month (1,2,...,12) and  $y$  represents the year (1,2,...,60). Monthly mean anomaly values are then formed, i.e.,

$$\hat{C}_{s,m} = \frac{1}{count_{s,m}} \sum_{y=1}^{60} C_{s,m,y} \varphi_{s,m,y}$$

where  $\varphi_{s,m,y}$  was equal to 1 if there was at least 1 observation at point  $(s,m,y)$  or 0 otherwise and  $count_{s,m}$  was defined as

$$count_{s,m} = \sum_{y=1}^{60} \varphi_{s,m,y}.$$

The null hypothesis that was tested was that the FSU climatology (1966-90) was the correct climatology for the period 1930-1989. If the FSU climatology is indeed the correct climatology for our period of interest, then the monthly anomaly mean values  $\hat{C}_{s,m}$  should zero. The null hypothesis can then be restated as the monthly mean anomaly values  $\hat{C}_{s,m}$  are zero. The

testing of the null hypothesis must then be done at each spatial position (1,2,...,2155) and month (1,2,...,12).

I first form a sample standard deviation  $SD$

$$SD_{s,m}^2 = \frac{1}{count_{s,m} - 1} \sum_{y=1}^{60} (C_{s,m,y} - \hat{C}_{s,m})^2.$$

Next, a test statistic  $t_{s,m}$  is calculated:

$$t_{s,m} = \frac{\hat{C}_{s,m} - \mu_0}{SD_{s,m} / \sqrt{count_{s,m}}}$$

where  $\mu_0$  is the desired mean (in this case 0).  $H_0$  can then be rejected if  $|t_{s,m}| > t_{\alpha/2}$ , where  $\alpha=.05$  and  $t_{\alpha/2}$  is based on  $count_{s,m}-1$  degrees of freedom.

## Appendix D

### *vector group renormalization*

Prior to developing the mathematics for Vector Group Renormalization (VGR), I first need to state two definitions. The product of the vectors  $A$  and  $B$  is defined as

$$\langle A, B \rangle = A^T \hat{H} B^* \quad (1)$$

and the modulus of  $C$  as

$$|C|^2 = \langle C, C \rangle$$

where  $\hat{H}$  is a diagonal matrix with weights  $\alpha^2$  ( $\alpha^2 \geq 0$ ) on the diagonal.

The fundamental idea of VGR is to take the vector set  $(M_1, M_2, M_3, \dots, M_N)$  and transform it into a new vector set  $(Q_1, Q_2, Q_3, \dots, Q_N)$  so that

$$\langle Q_n, Q_m \rangle = \delta_{n,m} \quad (2)$$

where  $\delta_{n,m}$  is Kronecker's delta. For  $Q_1$  let

$$Q_1 = \frac{M_1}{|M_1|}.$$

To find  $Q_2$  the below linear combination is first formed

$$R_2 = g_{2,1}Q_1 + M_2. \quad (3)$$

Next, the above equation is right multiplied by  $\hat{H}Q_1^*$ . I want

$$\langle R_2, Q_1 \rangle = 0,$$

i.e., I want the first and second vectors to be orthogonal. It can be shown that (3) reduces to

$$g_{2,1} \langle Q_1, Q_1 \rangle + \langle M_2, Q_1 \rangle = 0$$

and since  $\langle Q_1, Q_1 \rangle = 1$ , the following solution is obtained for  $g_{2,1}$ :

$$g_{2,1} = -\langle M_2, Q_1 \rangle.$$

$Q_2$  is obtained by normalizing  $R_2$  by its norm,

$$Q_2 = \frac{R_2}{|R_2|}.$$

To find  $Q_3$  I form the following linear combination

$$R_3 = g_{3,1}Q_1 + g_{3,2}Q_2 + M_3.$$

I now want

$$\langle R_3, Q_1 \rangle = 0$$

$$\langle R_3, Q_2 \rangle = 0,$$

i.e., I want  $Q_1$ ,  $Q_2$  and  $Q_3$  to be orthogonal. It can then show that

$$g_{3,1} = -\langle M_3, Q_1 \rangle$$

$$g_{3,2} = -\langle M_3, Q_2 \rangle.$$

$Q_3$  is obtained by normalizing  $R_3$  by its norm

$$Q_3 = \frac{R_3}{|R_3|}.$$

In general, to find  $Q_n$  ( $n > 1$ ), it can be shown that

$$R_n = g_{n,1}Q_1 + \dots + g_{n,n-1}Q_{n-1} + M_n$$

$$g_{n,m} = -\langle M_n, Q_m \rangle$$

$$Q_n = \frac{R_n}{|R_n|}.$$

## References

- Barnett, T. P., An attempt to verify some theories of El Niño, *J. Phys. Oceanogr.*, **7**, 633, 1977.
- Barnett, T. P., Prediction of the El Niño 1982-83, *Mon. Wea. Rev.*, **112**, 1403-1407, 1984.
- Bigg, G. R. and M. Inoue, Rossby waves and El Niño during 1935-46, *Q. J. R. Meteorol. Soc.*, **118**, 125-152, 1992.
- Busalacchi, A. J. and M. A. Cane, Hindcasts of sea level variations during the 1982-83 El Niño, *J. Phys. Oceanogr.*, **15**, 213-221, 1985.
- Busalacchi, A. J. and J. J. O'Brien, The seasonal variability in a model of the tropical Pacific, *J. Phys. Oceanogr.*, **10**, 1929-1951, 1980.
- Busalacchi, A. J. and J. J. O'Brien, Interannual variability of the equatorial Pacific in the 1960's, *J. Geophys. Res.*, **86**, 10,901-10,907, 1981.
- Busalacchi, A. J., K. Takeuchi and J. J. O'Brien, Interannual variability of the equatorial Pacific-revisited, *J. Geophys. Res.*, **88**, 155-195, 1983.
- Camerlengo, A. L., and J. J. O'Brien, Open boundary conditions in rotating fluids, *J. Comput. Phys.*, **35**, 12-35, 1980.
- Cane, M. A., Modelling sea level during El Niño, *J. Phys. Oceanogr.*, **14**, 1864-1974, 1984.



- Cane, M. A. and R. J. Patton, A numerical model for low-frequency equatorial dynamics, *J. Phys. Oceanogr.*, **14**, 1853-1863, 1984.
- Cane, M. A., S. E. Zebiak and S. C. Dolan, Experimental forecasts of El Niño, *Nature*, **321**, 827-832, 1986
- Cardone, V. J., Greenwood, J. G. and M. A. Cane, On trends in historical marine wind data, *J. Climate*, **3**, 113-127, 1990.
- Cooper, N. S., G. R. Bigg and K. D. B. Whysall, Recent decadal climate fluctuations in the tropical Pacific, *Int. J. Climatol.*, **9**, 221-242, 1989.
- Cressman, G. P., An operational objective analysis system, *Mon. Wea. Rev.*, **85**, 357-361, 1959.
- Diaz, H. F. and G. N. Kiladis, Atmospheric teleconnections associated with the extreme phases of the Southern Oscillation, *In* Diaz, H. F. and Markgraf, V. (eds.), *El Niño: Historical and Paleoclimatic Aspects of the Southern Oscillation*. Cambridge: Cambridge University Press, 7-28, 1992.
- Enfield, D. B., El Niño, past and present, *Rev. Geophys.*, **27**, 159-187, 1989.
- Enfield, D. B., Historical and prehistoric overview of El Niño/Southern Oscillation, *In* Diaz, H. F. and Markgraf, V. (eds.), *El Niño: Historical and Paleoclimatic Aspects of the Southern Oscillation*. Cambridge: Cambridge University Press, 95-117, 1992.
- Goldenberg, S. B. and J. J. O'Brien, Time and space variability of tropical Pacific wind stress, *Mon. Wea. Rev.*, **109**, 1190-1207, 1981.

- Inoue, M., and J. J. O'Brien, A forecasting model for the onset of a major El Niño, *Mon. Wea. Rev.*, **112**, 2,326-2,337, 1984.
- Johnson, M. A. and J. J. O'Brien, The northeast Pacific Ocean response to the 1982-1983 El Niño, *J. Geophys. Res.*, **95**, 7155-7166, 1990.
- Kiladis, G. N. and H. F. Diaz, Global climatic anomalies associated with extremes of the Southern Oscillation, *Journal of Climate*, **2**, 1069-1090, 1989.
- Kubota, M. and J. J. O'Brien, Variability of the Upper Tropical Pacific Ocean Model, *J. Geophys. Res.*, **93**, 13,930-13,940, 1988.
- O'Brien, J. J., Using supercomputers to understand and forecast El Niño, *I/O*, vol. 4, no. 2, 3-7, 1987.
- Oceanic Interdecadal Climate Variability, *IOC Technical Series 40*. UNESCO, 1992.
- Overland, J. E., and R. W. Preisendorfer, A significance test for principle components applied to a cyclone climatology, *Mon. Wea. Rev.*, **110**, 1-4, 1982.
- Posmentier, E. P., M. A. Cane and S. E. Zebiak, Tropical Pacific climate trends since 1960, *J. Climate*, **2**, 731-736, 1989.
- Quinn, W. H., V. T. Neal and S. E. Antunez de Mayolo, El Niño occurrences over the past four and a half centuries, *J. Geophys. Res.*, **92**, 14,449-14,461, 1987.
- Ramage, C. S., Secular change in reported surface wind speeds over the ocean, *J. Clim. Appl. Meteor.*, **26**, 525-528, 1987.
- Rasmusson, E. G. and T. H. Carpenter, Variations in tropical sea surface temperature and surface wind fields associated with the

- Southern Oscillation/El Niño, *Mon. Wea. Rev.*, **110**, 354-384, 1982.
- Shriver, J. F., M. A. Johnson and J. J. O'Brien, Analysis of remotely forced oceanic Rossby waves off California, *J. Geophys. Res.*, **96**, 749-757, 1991.
- Slutz, R. J., S. J. Lubker, J. D. Hiscox, S. D. Woodruff, R. L. Jenne, D. H. Joseph, P. M. Seurer and J. D. Elms, COADS-Comprehensive Ocean-Atmosphere Data Set, CIRES/ERL/NCAR/NCDC, Boulder, Colorado, 1985.
- Stricherz, J. N., D. M. Legler and J. J. O'Brien, Atlas of Florida State University tropical Pacific winds for TOGA 1966-1985, Florida State University, 1992.
- Trenberth, K. E., Recent observed interdecadal climate changes in the Northern Hemisphere, *Bulletin of the Amer. Meteor. Soc.*, **71**, 988-993, 1990.
- Whysall, K. D. B., N. S. Cooper and G. R. Bigg, Long-term changes in the tropical Pacific surface wind field, *Nature*, **327**, 216-219, 1987.
- Wyrtki, K., Sea level and seasonal fluctuations of the equatorial currents in the western Pacific Ocean, *J. Phys. Oceanogr.*, **4**, 91-103, 1974.
- Wyrtki, K., El Niño - The dynamic response of the equatorial Pacific ocean to atmospheric forcing, *J. Phys. Oceanogr.*, **5**, 572-584, 1975.
- Wyrtki, K. and G. Meyers, The trade wind field over the Pacific Ocean, *J. Appl. Meteor.*, **15**, 698-704, 1976.

Zebiak, S. E. and M. A. Cane, A model El Niño-Southern Oscillation,  
*Mon. Wea. Rev.*, **115**, 2262-2278, 1987.

### Biographical Sketch

Jay F. Shriver was born March 30, 1965 in Queens, New York. He earned a B.S. in mathematics and meteorology from the State University of New York, College at Brockport in 1987. He earned a M.S. in meteorology from the Florida State University in 1989 with Dr. J. J. O'Brien. His M.S. thesis, which was published in the *Journal of Geophysical Research - Oceans* in 1991, was titled "Analysis of remotely forced oceanic Rossby waves off California". Past honors include NASA Traineeship (1987-1989); membership in Chi Epsilon Pi Honor Society (1988); NASA Graduate Student Researchers Program (1990-1993); and session chair at the 1992 Fall AGU meeting. Mr. Shriver currently has a postdoctoral appointment with Dr. Harley Hurlburt at the Naval Research Laboratory, Stennis Space Center through a fellowship funded by the Office of Naval Technology.